SMC Bulletin

A Publication of the Society for Materials Chemistry

Volume 3 No. 2 August 2012

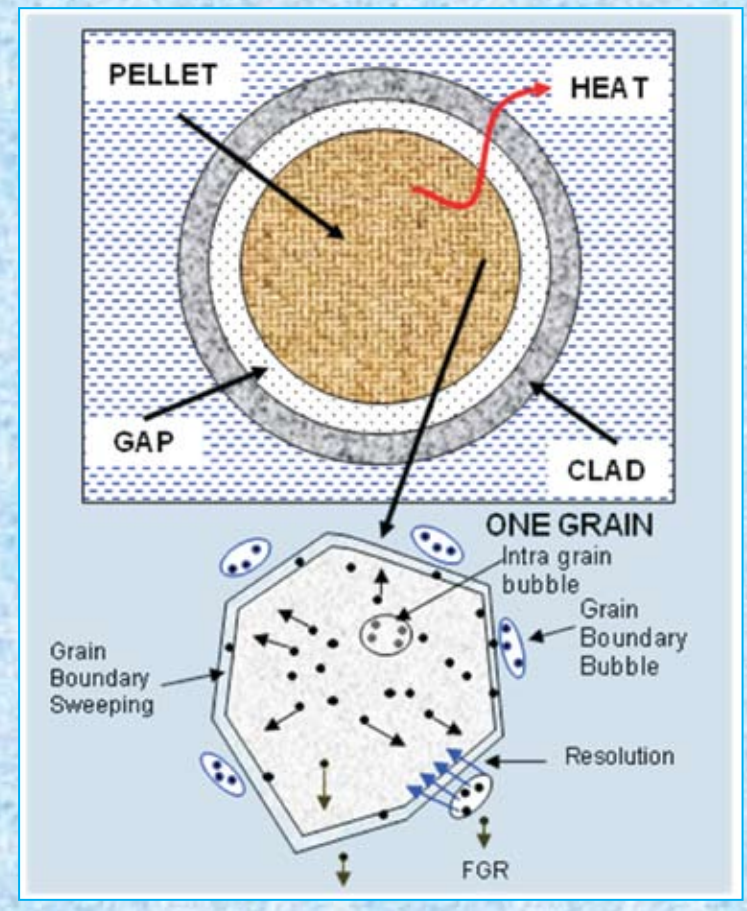

Thermophysical Properties of Nuclear Materials

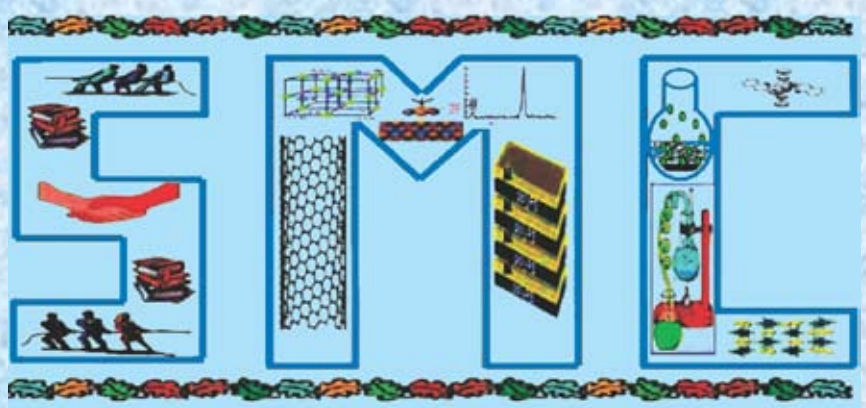

SOCIETY FOR MATERIALS CHEMISTRY

Society for Materials Chemistry was mooted in 2007 with following aims and objectives:

(a) to help the advancement, dissemination and application of the knowledge in the field of materials chemistry,

(b) to promote active interaction among all material scientists, bodies, institutions and industries interested in achieving the advancement, dissemination and application of the knowledge of materials chemistry,

(c) to disseminate information in the field of materials chemistry by publication of bulletins, reports, newsletters, journals.

(d) to provide a common platform to young researchers and active scientists by arranging seminars, lectures, workshops, conferences on current research topics in the area of materials chemistry,

(e) to provide financial and other assistance to needy deserving researchers for participation to present their work in symposia, conference, etc.

(f) to provide an incentive by way of cash awards to researchers for best thesis, best paper published in journal/ national/international conferences for the advancement of materials chemistry,

(g) to undertake and execute all other acts as mentioned in the constitution of SMC.

Executive Committee

SMC Bulletin

A Publication of the Society for Materials Chemistry

Volume 3 **No. 2** **August 2012**

Thermophysical Properties of Nuclear Materials

SOCIETY FOR MATERIALS CHEMISTRY

SMC Bulletin

Vol. 3, **No. 2** **August 2012**

Guest Editors

Shri Dheeraj Jain
Chemistry Division
Bhabha Atomic Research Centre
Trombay, Mumbai, 400 085
e-mail: jaind@barc.gov.in

Dr. Aparna Banerjee
Product Development Division
Bhabha Atomic Research Centre
Trombay, Mumbai, 400 085
e-mail: aparnab@barc.gov.in

Editorial Board

Published by
Society for Materials Chemistry
C/o. Chemistry Division
Bhabha Atomic Research Centre, Trombay, Mumbai, 400 085
E-mail: socmatchem@gmail.com,
Tel: +91-22-25592001

Front cover shows a schematic representation of fission gas release mechanism from a nuclear fuel pellet.

Guest Editorial

Dheeraj Jain

Aparna Banerjee

Nuclear materials used inside a reactor vessel or its peripheral components and sub-systems undergo variations in temperature from ambient to extreme levels upon irradiation. Therefore, information of its physical properties as a function of temperature becomes very important. The main thermophysical properties desired by nuclear scientists and engineers working in the field of reactor development are thermal conductivity, thermal expansivity, specific heat capacity, thermal radiative properties, thermo-elastic properties, viscosity, surface tension, chemical diffusion and sound velocity in materials. The nuclear materials for which these properties are required include fuel matrix with and without fission products, clad, control rods, coolants, coolant channels, pressure tubes, structural materials, etc. Precise and accurate information of these properties for understanding the performance of different components is therefore very essential.

The field of studying thermophysical properties of nuclear materials has been extensively explored by scientists across the globe and still continues to be an importnat wing in science and technology of reactor development. It is therefore relavent to bring out a compilation of few articles from experts working in this field in the form of a theme-based issue of SMC bulletin for all the members of society and other readers with their interest in the field of materials chemistry.

The topics covered in this issue, on one hand, give an overall perspective of the importance of themophysical properties of nuclear fuels to predict the fuel performance inside a reactor. On the other hand, the potential of modern computational methods for predicting the thermophysical properties of advanced fuels such as plutonium bearing oxides, nitrides and carbides, for which experimental database is scarcely avilable as well as difficult to generate, is presented. The phenomenon of diffusion in ceramic nuclear fuels, which plays an important role during fuel fabrication and its irradiation inside the reactor is covered in one of the article with underlying basics and relevant examples. Two articles have provided emphases on thermophysical properties of glasses and glass-ceramics, which are potential candidates for either nuclear waste immobilization or high temperature sealing applications. Results on structural and bulk thermal expansion behavior of thoria-based fuels, which are candidate fuels for Indian Advanced Heavy Water Reactor (AHWR) are also presented.

It is indeed our privilage to thank all the contributors, who have, within a short notice, agreed to our request and provided their articles for this issue by spending their valuable time. We also would like to thank the editorial committee of SMC bulletin for inviting us as guest editors of this issue. Finally we hope that the readers would find this theme-based issue interesting and useful.

Editorial Note

We are very happy to present the fourth issue of SMC bulletin, based on a very important theme, "Thermophysical properties of Nuclear Materials". It was the collective decision of our team to invite researchers working in respective fields as guest editors of such theme-based issues of SMC bulletin as this would provide a better focus to the central theme and therefore would benefit our members and other readers in a better way. We are thankful to both the guest editors, Dheeraj Jain and Aparna Banerjee, who have spared their valuable time in a well coordinated way to bring out this bulletin in time.

We hope that our readers would find the contents quite interesting and useful and would provide us their feedback so as to enable us in further improving the SMC bulletin.

The next issue of the bulletin is proposed to be based on the theme: Fuel Cell Materials. Readers are invited to contribute their theme-based articles for this forthcoming issue.

Editors

From the President's Desk

Dear Fellow members,

It is really satisfying to note that the Society for Materials Chemistry (SMC) has initiated the publication of theme-based issues of SMC bulletin. This would benefit all our members and other readers by providing articles from experts working in the related fields around a central theme. Such theme-based issues would also encourage other young researchers and academicians to join this fast growing society, having more than 550 life members in a short span of time. A very important occasion for all of our members and other new aspirants is nearing as the society is organizing its 4th biennial symposium, "Interdisciplinary Symposium on Materials Chemistry (ISMC-2012)" in BARC, Mumbai during December 11-15, 2012. Members are invited to send their research results in the form of abstracts and participate in the symposium.

The theme of this issue of SMC bulletin, "Thermophysical Properties of Nuclear Materials" is a very relevant one covering nearly all the topics in this field and the very important role of materials chemistry in developing desired materials for the intended applications. I expect, that the bulletin, in form of these theme-based issues will continue to serve as a platform to highlight the advances made in the field of materials chemistry and will also get constructive feedback from our members. Members are once again encouraged to send a brief note on major instrumental facilities available in their institutes and also major awards and achievements received.

T. Mukherjee

CONTENTS

Feature Articles

A compilation of required thermo-physical properties of advanced fuel for in-pile prediction of fuel performance

B.K. Dutta
Reactor Safety Division
Bhabha Atomic Research Centre, Trombay, Mumbai-400 085.
E-mail: bkdutta@barc.gov.in

Introduction

The fuel performance analysis code 'FAIR' was developed to analyse performance of the uranium-based {UO_2 & $(U,Pu)O_2$} fuel under normal operating and accidental conditions. To enhance the capability of this code so as to analyze advanced fuel, such as thorium-based fuel, it is necessary to generate a number of properties. In this article, such properties are listed under following three headings:

1. Properties related to thermal analysis
2. Properties related to deformation analysis
3. Properties related to fission gas release.

The expressions used in the 'FAIR' code for different properties of uranium-based fuel are also shown for ready reference. The thermal analysis, deformation analysis and fission gas release modules are interdependent on each other as shown below in fig. 1.

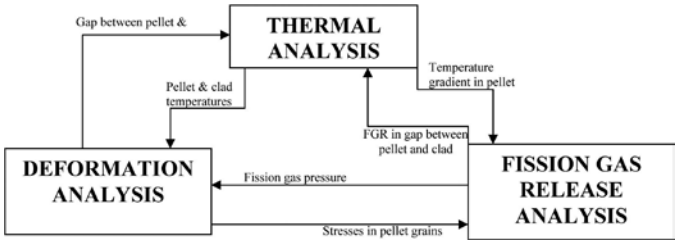

Fig.1 Interdependency between three modules of fuel performance code

Properties Related to Thermal Analysis

Burn-up Dependent Thermal Conductivity

This property (λ) is used in code 'FAIR' to calculate steady state as well as transient temperature distribution in the pellets. The thermal conductivity of irradiated UO_2 is given by SIMFUEL correlation. The SIMFUEL correlation is given by

$$\lambda = [0.053 + (0.016 \pm 0.0015)bu] + [2.2 - (0.005 \pm 0.002)bu] \times 10^{-4} T$$

Where, 'bu' is the burnup in atom%, 'T' is temperature in Kelvin and 'λ' is the thermal conductivity of UO_2 in W $m^{-1} K^{-1}$.

Specific Heat

This property is used in code 'FAIR' for calculating transient temperature distribution in the pellet. For the case of UO_2 and PuO_2, this property is given as a function of temperature, composition, molten fraction and oxygen to metal (O/M) ratio.

$$C_p = K_1\theta^2 \exp(\theta/T)/[T^2(\exp(\theta/T) - 1)^2] + K_2T + (OMR/2)(K_3E_D/RT^2)\exp(-E_D/RT)$$

where,

C_p = specific heat capacity (J $Kg^{-1}K^{-1}$)

T = Temperature (K)

OMR = oxygen to metal ratio

R = Universal gas constant = 8.3143 (J $mol^{-1}K^{-1}$)

θ = The Einstein Temperature (K)

K_1 to K_3, θ and E_D = constants given separately for UO_2 and PuO_2

Properties Related to Deformation Analysis

Thermal Expansion

This property is used in code 'FAIR' to predict changes in pellet geometry due to temperature change. Linear thermal expansion models are available for both UO_2 and $(U,Pu)O_2$ fuel and are given below for the reference. The expansion of solid mixed oxides is calculated from the weighted average of the expansion for UO_2 and that of PuO_2.

i. UO_2 Solid Phase:

$$\Delta L/L = -4.972 \times 10^{-4} + 7.107 \times 10^{-6} T + 2.581 \times 10^{-9} T^2 + 1.140 \times 10^{-13} T^3$$

ii. UO_2 Phase Change at Melting Point (T_m):

$$\Delta L/L = \Delta L/L(T_m) + 3.096 \times 10^{-2} R$$

iii. UO_2 Liquid Phase:

$$\Delta L/L = \Delta L/L(T_m) + 3.096 \times 10^{-2} R + 3.5 \times 10^{-5}(T - T_m)$$

iv. $(U,Pu)O_2$ Solid Phase:

$$\Delta L/L = -3.9735 \times 10^{-4} + 3.4955 \times 10^{-6} T + 2.1513 \times 10^{-9} T^2 + 3.7143 \times 10^{-16} T^3$$

Modulus of Elasticity (E)

This is required in code 'FAIR' to calculate deformation and stresses in the pellet. For ceramic fuel, this is affected by temperature, density and to a lesser extent by oxygen to metal ratio (O/M) and burn-up.

i) For stoichiometric UO_2 fuel, below melting temperature:

$E_s = 2.334 \times 10^{11}[1.0 - 2.752(1.0 - D)].[1.0 - 1.0915 \times 10^{-4}T]$

ii) For non-stoichiometric fuel or fuel which contains PuO_2

$E = E_s exp(-Bx)(1.0 + 0.05f)$

Where, D is the density, B is the burn-up.

Poisson's Ratio (ν)

This property is also required to calculate fuel deformation and stresses. It is related with modulus of elasticity and shear modulus as follows:

$\nu = E/2G - 1$

Where, 'E' is Modulus of elasticity and 'G' is Shear Modulus

Thermal Creep

This property is used in code 'FAIR' to calculate pellet deformation and stresses. This is generally modelled as a function of time, temperature, grain size, density, fission rate, oxygen to metal ratio and external stresses. For UO_2 or mixed oxide fuels, a transition stress is defined at which creep rate changes from "linear stress dependence" to a creep rate proportional to "stress to the power 'n'".

The steady state creep rate (ε_s) of UO_2 is determined using the following relations:

$\varepsilon_s = \{(A_1 + A_2F)\sigma exp(-Q_1/RT)\}/\{(A_3 + D)G^2\} + \{A_4 + A_5F)\sigma^{4.5} exp(-Q_2/RT)\}/\{A_6 + D\} + A_7\sigma F\ exp(Q_3/RT)$

where, A_1 to A_7 are constants, 'F' is fission rate, 'Q_1 to Q_3' are activation energies, 'σ' is the stress, 'R' is the universal gas constant, 'T' is the temperature in Kelvin, 'G' is shear modulus, 'D' is density

For mixed oxide, the steady state creep rate is given by

$\varepsilon_s = \{(B_1 + B_2F)\sigma exp[-Q_3/RT + B_3(1-D) + B_4C]\}/G^2 + \{B_5 + B_6F)\sigma^{4.5} exp[-Q_4/RT + B_7(1-D) + B_8C]$

where, B_1 to B_8 are constants, 'F' is fission rate, 'Q_3 to Q_4' are activation energies, 'σ' is stress, 'R' is the universal gas constant, 'T' is the temperature in Kelvin, 'G' is shear modulus, 'D' is density.

Densification

This property is required in code 'FAIR' to calculate fuel dimensional changes during initial irradiation of the pellets. In case of UO_2 and $(U,Pu)O_2$ fuels during the first few thousand hours, the densification is calculated as a function of fuel burn-up, temperature and initial density. Densification as a function of burn-up is calculated using the following equation:

$(\Delta L/L) = (\Delta L/L)_m + exp\{-3(FBU + B)\} + 2.0\ exp\{-35(FBU + B)\}$

Where, '$(\Delta L/L)$' is dimensional change in %, '$(\Delta L/L)_m$ is the maximum possible dimension change of fuel due to irradiation in %, 'FBU' is the fuel burn up in MWd/kGU, 'B' is a constant to suit the boundary condition: $\Delta L/L = 0$ for FBU = 0.

Fuel Swelling

This property is required in code 'FAIR' to calculate pellet deformation, which in turn affects Pellet-Clad interaction. Fuel swelling results from the increased volume of fission products. It is defined as a positive volume change due to different solubilities, chemical states, lattice parameters, numbers of atoms, and chemical valancies of the atoms resulting from the nuclear fission process.

In case of UO_2, swelling due to solid fission product is given by:

$S_s = 2.5 \times 10^{-29} B_s$

The correlation for swelling due to gaseous fission products (for T < 2800 K):

$S_g = 8.8\ X\ 10^{-56}\ (2800-T)^{11.73}\ exp[-0.0162\ (\ 2800-T)]\ exp(-8.0X10^{-27}B)B_s$

where, 'S_s' is the fractional volume change due to solid fission products, 'B_s' is burn-up during a time step (fissions/m^3), 'S_g' is the fractional volume change due to gaseous fission products, 'B' is the total burn-up of the fuel (fission/m^3) and 'T' is the temperature (K).

Fuel Fracture Strength

This property is used in code 'FAIR' to consider pellet cracking in Finite Element Model. In case of UO_2-based fuel, fracture strength is a function of density and temperature up to 1000 K. Beyond 1000 K, a constant value is used. The following relation is given for the temperature up to 1000 K.

$$\sigma_F = 1.7 \times 10^8 [1.0 - 2.62(1.0 - D)]^{0.5} \exp(-1590/8.314T)$$

Where, 'D' is the density and 'T' is the temperature (K).

Above 1000 K, the fracture strength is taken as $\sigma_F = \sigma_F$ (1000K).

Properties Related To Fission Gas Release

Thermal Release

The fission gas release (FGR) in the code 'FAIR' is calculated using physically-based model. The model assumes the transfer of gas atoms from the grain matrix to the grain boundaries is due to (i) diffusion and (ii) grain boundary sweeping. The gas atoms may be transferred back to the grain matrix from the grain boundaries due to 'irradiation induced re-solution'. The effects of these three mechanisms (i.e., diffusion, sweeping and re-solution) lead to net accumulation of gas atoms at the grain boundaries. The grain boundaries have a limited capacity to hold the gas atoms in bubbles. During the initial period of irradiation, atoms remain at the grain boundaries in bubbles. Once the capacity of the grain boundaries is saturated, the further transferred gas atoms are released as free atoms to the various cracks, voids, fissures, etc. Fig. 2 pictorially explains the fission gas release mechanisms discussed above. Fig. 3 shows the block diagram of the same mechanism used to develop the module.

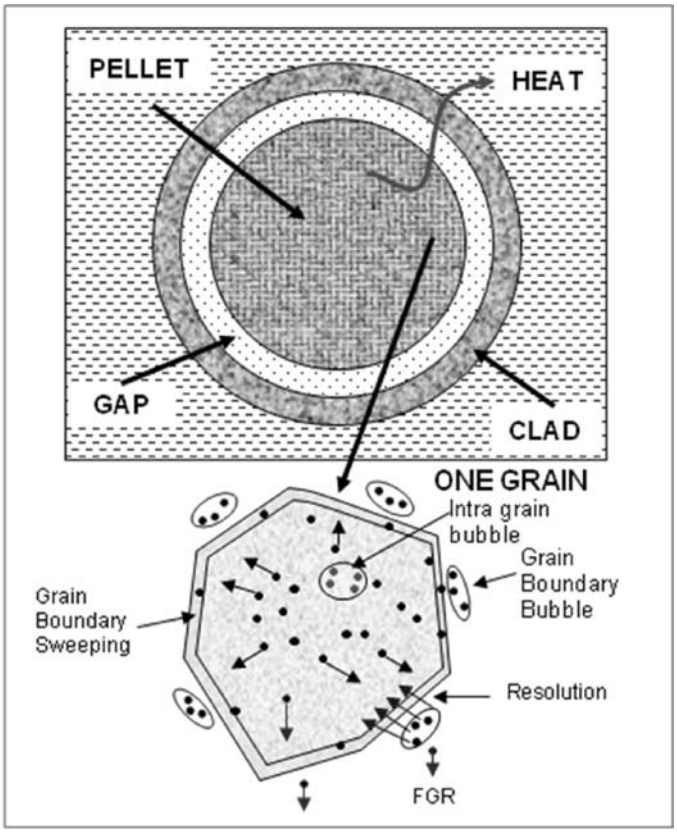

Fig.2 Fission gas Release Mechanism: A Pictorial View

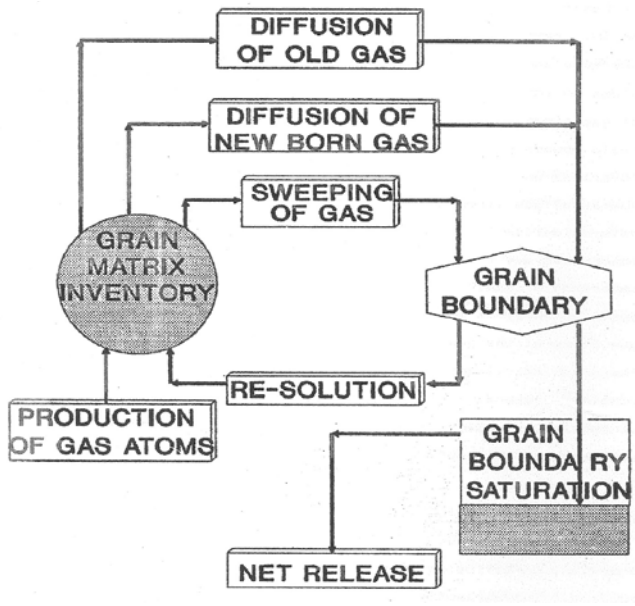

Fig. 3 Fission Gas Release Mechanisms: Block Diagram

A. Single Atom Diffusion Coefficient:

The single atom diffusion coefficient is expressed as

$$D = 7.6 \times 10^{-10} \exp\left(-2.9289 \times \frac{10^5}{RT_k}\right) + s^2 j_v V + 2 \times 10^{-40} F$$

where,

$$j_v = 10^{19} exp(-23097 \times \frac{10^5}{RT_k})$$

$$V = \frac{\alpha_s s^2 + ZV_0}{2Z}\left[\left(1 + \frac{4K'Z}{j_v(\alpha_s s^2 + ZV_0)^2}\right)^{-1} - 1\right]$$

$$V_0 = \exp\left(-2.3097 \times \frac{10^5}{RT_k}\right)$$

Here, $s = (4.09 \times 10^{-29})^{2/3}$; $\alpha_s = 10^{15}$; $Z = 2$; $K' = 10^4$, F = fission rate (fissions/m^3-s)

B. Effective Diffusion Coefficient

The above shown single atom diffusion coefficient should be modified to take care of trapping of the gas atoms within intra-granular bubbles. Such gas atoms are unable to take part in further diffusion unless these are released from the intra-granular bubbles. Hence effective diffusion coefficient has been found to be less than the single atom diffusion coefficient. This is given as follows:

$$D' = \frac{Db}{b + g}$$

Where, 'b' is re-solution rate of trapped gases in bubbles back into matrix and 'g' is trapping probability at bubbles.

C. Grain Growth

This is an important model used in the code 'FAIR' to calculate fission gas release to the grain boundary due to

grain boundary sweeping. The grain growth is a function of temperature, initial grain size and time. In case of UO_2-based fuels, equiaxed grain growth is given by

$$d^4 - d_0^4 = 1.717 \times 10^{10} \exp\left(-3.87 \times \frac{10^5}{RT_k}\right) t$$

Where, 'd' is the final grain diameter (μm), 'd_o' is the initial grain diameter (μm), 'R' is the universal gas constant (in J/mol-K), 'T' is the temperature (K) and 't' is the time (s).

D. Irradiation Induced Re-solution

The gas atoms stored in inter granular bubbles have a tendency to enter back into the grain matrix by a process, called re-solution. The gas atoms which enter back the matrix are concentrated in a very narrow region near the grain boundary. Further gas atom diffusion is possible only when the density of gas atoms in the matrix overcomes this barrier. The number of gas atoms re-entering the grain matrix due to re-solution is given by

$$N_{res} = \frac{bN_{gb}}{2}$$

The threshold barrier concentration is given by

$$C_{maxm} = \frac{b\lambda N_{gb}}{2D'}$$

Where, 'N_{res}' is number of atoms entering back into the grain matrix due to re-solution (atoms/m^2-s), 'b' is the irradiation induced re-solution rate of gas atoms at the grain boundary back into the matrix, 'N_{gb}' is density of atoms on the grain boundary (atoms/m^2), 'λ' is the re-solution depth and 'D' is effective diffusion coefficient.

E. Grain Boundary Saturation Limit

The grain boundary saturation limit is a function of temperature, surface energy and external mechanical constraint. The saturation limit is obtained by balancing the pressure inside the inter granular bubbles against the capillary forces restraining the bubble in addition to the mechanical forces operating on the bubble. The maximum grain boundary capacity is given by

$$N_f^{max} = C_i \frac{4\pi r_f^2}{3KTsin^2(\theta)} f_f(\Theta) f_b \left[\frac{2\gamma}{r_f} + P_{ext}\right]$$

Where, 'N_f^{max}' is grain boundary saturation limit (atoms/m^2), 'C_i' is fission yield of an isotope (ton of isotope/MWd), 'r_f' is radium of grain face bubble (~0.5 x 10^{-6} m), 'K' is Boltzmann's constant, 'T' is the temperature (K), 'θ' is the semi di-hedral angle (~50°), '$f_f(\theta)$' is ratio of volume of lens to that of sphere, 'f_b' is fractional coverage of grains by lenticular bubbles (~0.5), 'γ' is free surface energy (~626 x 10^{-9} J/m^2) and 'P_{ext}' is external force.

Athermal Release

At low temperature, gas atoms are released due to irradiation from the surface of the fuel. Such release does not depend upon the temperature of the fuel. The athermal release rate used in code 'FAIR' is given by

$$f_{low} = C_2 \times \frac{S}{V} \times B_u$$

Where, 'C_2' is proportionality constant for athermal release (1.17 x 10^{-6} t/MWd-m), 'S' is geometric surface area of the pellet (m^2), 'V' is the volume of the pellet (m^3) and 'B_u' is the burn-up (MWd/TeU).

Caesium and Iodine Release Model

This model is used in the code 'FAIR' to calculate caesium and iodine release with burnup of the fuel. The caesium and iodine release data is used to check any possibility of crack initiation and crack propagation, which may ultimately lead to clad rupture. These releases are modelled separately for each isotope since the decay rate of the different isotopes requires separate treatments. Moreover, the approximation used to model long-and short-lived isotopes are different. Long-lived isotopes accumulate in the fuel in proportion to the burn-up and are released by diffusion. Short-lived isotopes achieve a steady state in which their rate of release to the fuel rod pellet-cladding gap. The concentration of short-lived isotopes is proportional to the rate of burn-up. In case of UO_2-based fuels, the expression for long-lived iodine and caesium isotopes release is given as follows:

For the long lived isotopes of Iodine (I^{127}, I^{129}), the expression used to predict the release of isotope to the fuel rod free volume is

$$R_i = C_i B_u \left[\frac{4}{a_I}\left(D_I \frac{t}{\pi}\right)^{\frac{1}{2}} - \frac{3}{2} D_I \frac{t_z}{a_I}\right]$$

$$D_I = 6.6 \times 10^{-6} \exp\left(-\frac{36086}{T_k}\right) \quad for\ T_k > 1134.054\ K$$

$$= 10^{-19} \quad for\ T_k \le 1134.054\ K$$

$$a_I = 3[T_D] \times 10^{[20.61 - T_D(67.9 - 46T_D)]}$$

Where, 'R_i' is specific isotope yield (kg of isotope/kg of fuel), 'C_i' is fission yield of isotope (Ton of isotope/MWd), 'B_u' is burn-up (MWd/TeU) and 'a_I' is diffusion distance for gas release (m).

Analysis of a Fuel Pin Subjected to Power Pulse

To demonstrate the usefulness of a fuel performance code to predict in-pile fuel behaviour under normal operating as well as accidental conditions, a case study is shown below. The case study deals with the analysis of a fuel pin up having seen high burn-up is then subjected to a major power pulse. The code 'FAIR' was used to predict the fuel performance parameters as a part of IAEA exercise. The results predicted by different codes worldwide were compared with the test results. The details are as follows:

Salient Features of the Tests (information as received from IAEA)

The rod FK-1was re-fabricated from irradiated segment fuel rods of BWR 8x8 BJ (STEP I) design. The segment was irradiated to an assembly average burn-up of 30.4 MWd/kgU in Fukushima Daiichi Nuclear Power Station Unit-3. Before re-fabricating, the whole fuel rod was examined by Visual observation, X-Ray radiography, Eddy current testing, Dimensional measurements, oxide thickness measurement, Gamma scanning and Fission gas sampling.

The test was conducted on sections of fuel stack ~106 mm long, chosen to have a flat axial burn-up profile. An iron core was placed in the top end fitting to measure fuel stack elongation and an internal pressure sensor was built into the bottom fitting. Hafnium disks were placed at both ends of the fuel column to prevent power peaking and the rods sealed with 0.3 MPa helium gas corresponding to the original filling conditions. Prior to the test, each rod was subjected to the various examinations, such as, Helium leak test, Visual observation, X-Ray radiography, Eddy current testing, Dimensional measurement, weight measurement and Gamma scanning.

Two sheathed thermocouples were attached to each sample and mounted 10 mm distant from the cladding to measure coolant temperature. Three small diameter thermocouples (0.2 mm) were spot welded to the outside cladding of FK-1 to measure clad temperatures.

The pulse irradiation of FK-1 was carried out on November 21, 1996. The reactor power arose at about 0.20 s. The pulse width (full width at half maximum) was 4.4 ms. The peak fuel enthalpy was evaluated to be 544 J/g (130 Cal/g). The various parameters measured during the tests are coolant temperature, clad temperature, elongation of fuel stack and cladding and rod internal pressure.

Analysis Using Code FAIR

As a part of FUMEX-III CRP exercise of IAEA, the case was analyzed using code 'FAIR'. The input data on fuel beside finite element mesh data is shown below:

Pellet Inner Radius (mm):	0.000
Pellet Outer Radius (mm):	5.155
Pellet Height (mm):	10.00
Initial Gap (mm):	0.120
Plenum Volume (mm3/mm):	16.66
Pellet Surface Roughness(mm):	0.00160
Filled Gas Type:	HELIUM
Filled Gas Pressure (MPa):	0.300
Filled Gas Temperature (degK)	300.00
Conductivity Equation (SIMFUEL/MATPRO/THORIUM):	SIMFUEL
Basic Fuel (Uranium/Thorium):	URANIUM
U235/U233 Fraction (ENRICHMENT):	0.0340
Fast Flux Factor:	0.975
Resonance Escape Probability:	0.920
Fuel Fabricated Density (gm/cm3):	10.431
Weight Percent of Plutonium:	0.000
Maximum Density by Densification (gm/cm3):	10.5506
Sintering Temperature (deg.K)	1923.0
Open Porosity (%)	1.0
Density Change during Sintering (g/cm3) (=0 if not known)	0
Initial Fuel Grain Size:(micron)	8.000
Consider Athermal FGR??	Y
Consider HBS FGR??	Y
Fraction of Fuel Relocation:	0.450
Min. Linear Power for relocation (w/mm)	7.500
Correction factor on linear power:	1.00492454
History number at which refabrication done	12700
Gas filled during refabrication	HELIUM
Gas pressure during refabrication (Mpa)	0.300
Gas temp during refabrication (deg.K)	293.15
Plenum volume after refabrication(mm3/mm)	5.000
History number at the start of power pulse	13710
History number at the end of power pulse	14100
Clad Surface Roughness (mm):	0.00160

The computed results are temperature, stresses and fission gas release during base irradiation and same set of parameters during power pulse. The results are shown in Fig.4. The same figure also shows the comparison of clad temperature with the measured values.

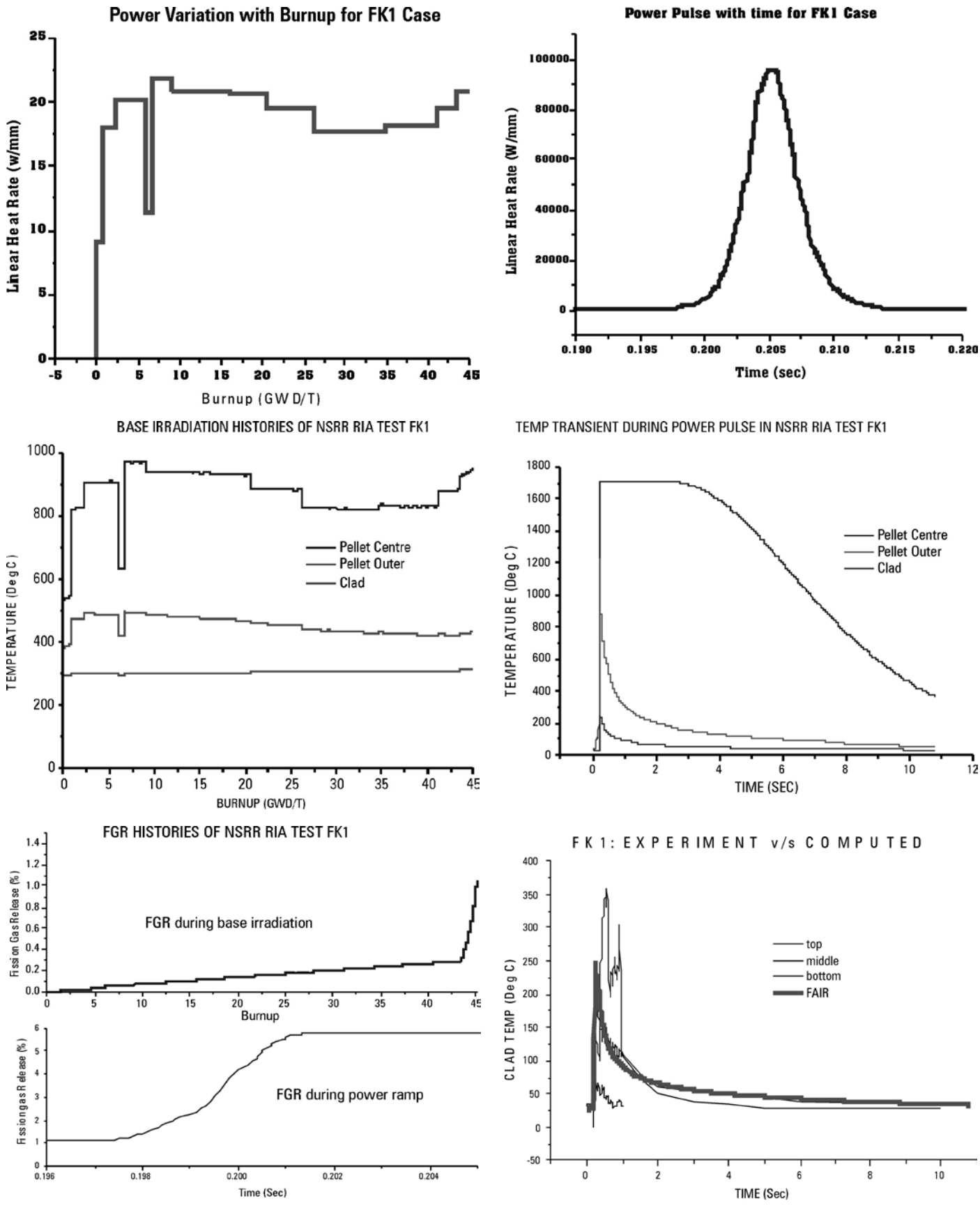

Fig.4 Results of Analysis of a Fuel Pin Subjected to Power Pulse Using Code FAIR

Conclusions

The present paper summarizes all the thermo-physical parameters required for an advanced fuel. Parameters are required to carry out in-pile prediction of fuel performance under various power transients. Similar parameters and their form of equations are shown for UO_2 fuel for better understanding of mathematical form of these parameters. A case study is shown to demonstrate importance of such fuel analysis codes.

B.K. Dutta, *Distinguished Scientist, BARC is associated with the development of a fuel performance code FAIR. The code participated in three IAEA CRPs on 'Modelling of fuel pins at extended burn-up'. He has also modified the code to model Triso particles of CHTR up to a very high burn-up. Presently he has interest to modify the code to model thoria-based advanced fuel. He is also involved in Indo-UK project on 'Fundamental properties of thoria-based mixed oxides', funded by EPSRC, UK.*

Diffusion in nuclear ceramic fuels

T.R. Govindan Kutty
Formerly from Radiometallurgy Division,
BARC, Trombay, Mumbai - 400 085.
Email: trgkutty@yahoo.com

Introduction

Atomic diffusion is a very important basic process controlling many phenomena during fabrication and irradiation of the nuclear fuels. For example, mass transport governs the densification process during sintering. The processes like grain growth, creep, fission gas bubble formation and their migration, and fission gas release, etc. are also controlled by diffusion [1-3]. All these processes are related to metal atom diffusion, since in all of the ceramic fuels the metal atoms diffuse at much lower rates than the non-metal atoms (oxygen, carbon, nitrogen). The slower species is normally rate-controlling, since for true matter transport to occur, all of the components of a compound have to be transported. To understand fully the diffusion processes, their dependences on deviations from stoichiometry, on impurities, etc. should all be known. In addition, at temperatures below about $0.5T_m$, (T_m, is the melting point in Kelvin), direct enhancement of diffusion by radiation and by the fission events has to be considered. An outstanding challenge in the design and manufacturing of nuclear fuels is to achieve the required density with acceptable microstructure while maintaining structural integrity. Sintering of oxide, nitride, and carbide fuel pellets requires a strict control of composition, thermal treatment, pressure, and atmosphere [4-6]. In this paper, the importance of diffusion in the fabrication of nuclear fuel is described with the help of experimental results.

Fundamentals of diffusion

Diffusion is the transport of matter, in the form of atoms, ions or molecules and is responsible for most structural changes. Diffusion process is described through Fick's first law [1, 3]:

$$J = -D(dC/dx) \quad (1)$$

where J is the flux of a species in moles per unit area per unit time, D is the diffusion coefficient and dC/dx is a concentration gradient. D is a useful property of materials, since it describes the rate of diffusion of a species, or its diffusivity and usually appears in units of cm^2/s. To measure the diffusion coefficient, Fick's first law requires a fixed concentration gradient, a condition difficult to establish experimentally. It is more convenient to measure the change in concentration with time which is commonly known as Fick's second law

$$\delta C/\delta t = D\,(\delta^2 C/\delta x^2) \quad (2)$$

Types of Diffusion Coefficients

Although the single symbol D has been used to denote the diffusion coefficient, there are several variants of diffusion coefficients [1-4]. They are classified as follows:

a) The self diffusion coefficient, D^{self}

This property refers to the migration of the atoms of a pure element or the cation or anion of an ionic solid in the absence of a concentration gradient. There is no direct method for measuring the self-diffusion coefficient.

b) The tracer diffusion coefficient, D^{tr}

This diffusivity is subject to the same conditions as the self-diffusion coefficient except that some of the atoms are radioactive isotopes of the host element or ion. Measurement of D^{tr} requires a gradient of the tracer but there is no gradient or flux of the combined radioactive and nonradioactive element or ion. The diffusivities of these two forms are equal.

c) The Intrinsic Diffusion coefficient, D^{In}

This quantity refers to the diffusion of a species in a binary solid. Each species possesses an intrinsic diffusion coefficient, designated as D_A^{In} and D_B^{In} for the components A and B respectively. Intrinsic diffusivities could also refer, for example, to U^{4+} and Pu^{4+}, interdiffusing in the mixed oxide $(U,Pu)O_2$. The intrinsic diffusivities of the components of a binary solid are in general not equal. These diffusivities imply concentration gradients of the species A and B, in contrast to the gradient-free self and tracer diffusion coefficients. In preparing the couple of two solids, the interface is "marked" by placing a series of inert metal wires between the two blocks. During the diffusion anneal, the markers are found to move relative to the stationary ends of the couple. This fact implies that the two species do not migrate at the same rates, or that they have different intrinsic diffusion coefficients. Both species obey Fick's law with the moving marker interface as the origin of the distance x.

d. The Mutual Diffusion Coefficient, $\widetilde{D}$

This type of diffusion coefficient is also called the chemical or inter-diffusion coefficient. It is closely related to the marker experiment. Measurement of the A-B concentration gradient relative to the fixed ends of the diffusion couple (rather than relative to the marker wires) produces $\widetilde{D}$. The intrinsic diffusivities and the mutual diffusion coefficient are related by the so-called Darken equation:

$$\widetilde{D} = x_B D_A^{In} + x_A D_B^{In} \quad (3)$$

Diffusion in Ionic Crystals

Diffusion in ionic crystals differs from that of metals in numerous ways [1, 3]:

1. Ionic solids contain at least two components which are oppositely charged.
2. Cations and anions generally exhibit very large differences in intrinsic diffusivities; sometimes as large as seven orders of magnitude.
3. The type of defect that predominates (Schottky or Frenkel) controls the magnitudes of the diffusivities.
4. The effect of substitutional doping of ionic solids with cations of different valence from the host cation has a profound effect on the diffusivities, often of both ions.
5. The requirement of local electrical neutrality affects the movement of the ions.
6. Interstitial impurity diffusion is not as important in ionic solids as it is in metals and other elements.

All four mechanisms are not operative in a particular ionic solid. The mechanism that dominates for the cations may be different from that controlling anion motion.

Diffusion in UO_2

Diffusion in uranium dioxide is of greater importance and substantially more complicated than in the NaCl example reviewed in the preceding section.

1. Diffusivities of the anion (oxygen) and the cation (uranium), although very different in magnitude, are both technologically important.
2. Diffusion of impurity species, both ionic and neutral, influence the behavior of nuclear fuel.
3. Multiplicity of uranium oxidation states permits extrinsic point defects to control the diffusivity: U^{5+} is effectively a dopant on the cation sub-lattice.
4. Intrinsic point defects, important around exact stoichiometry, are controlled by both anion Frenkel and Schottky processes. Although the migration of the ions is restricted to their proper sub-lattices, the point defect equilibrium involving one component can affect the point defect concentration, and hence the diffusivity, on the other sub-lattice [4-7].

Diffusion in sintering

The sintering process is diffusion controlled one whose rate is controlled by the slower moving metal atoms. The ratio of oxygen diffusion coefficient and uranium diffusion coefficient, D^O/D^U, is reported to be greater than 10^5 at 1400°C, suggesting that the uranium ion mobility is much smaller than the oxygen mobility. In fact, D^U increases in proportion to x^2 by about 5 orders of magnitude between UO_2 and $UO_{2.2}$ at 1400-1600°C.The point defect model has been used to explain many observed features of diffusion in non-stoichiometric fluorite type oxide fuels [5].

Point defect model

The point defect model attributes the observed changes in metal atom diffusion coefficient solely to the change in the point defect concentration brought about by the deviation of x from the stoichiometry while varying the oxygen potential. The point defect model was first developed by Matzke [8] and Lidiard [9]. Deviations from stoichiometry produce point defects, most likely oxygen vacancies or metal interstitials in hypo-stoichiometric compounds and oxygen interstitials or metal vacancies in hyper-stoichiometric compounds. The point defects are also created thermally in these materials, provided the temperature is high enough. These defects can exist as single, isolated point defects at low concentration. At higher concentrations, the defects will aggregate into clusters, will become ordered or will be eliminated by the formation of two or three dimensional defects such as dislocation loops, shear planes, voids, etc. [6-9]. A relation has been derived for the temperature dependence of the concentration of vacancies and interstitials in both the oxygen and metal sub-lattice by solving the anion Frenkel, Schottky and cation Frenkel defects (Table 1) [10-13]. The uranium vacancy and uranium interstitial concentrations are calculated using the relations given in Table 1 for stoichiometric and non-stoichiometric compositions [13]. The concentrations of uranium vacancies are plotted against O/U ratio for various temperatures in Fig. 1 [8]. The figure shows that there is a drastic change in the uranium vacancy concentration on varying O/U around the stoichiometric composition.

Parameters affecting sintering

Temperature is the powerful parameter that can enormously influence sintering rates. It is possible to estimate a good sintering temperature for a material just by knowing its diffusivity: A good first guess for the sintering temperature is that for which the effective diffusion distance is roughly equal to the mean particle size [14-16]. If the diffusivity is not known for a particular material, then a rough estimate of sintering temperature can be taken as ~ 7080% of the melting temperature. Finally, to increase sintering rates one can think of decreasing the mean particle size. Decreasing the particle size will decrease the effective diffusion distances necessary to achieve the same microstructural changes.

The distance over which appreciable diffusion can occur in a given time interval is:

$$X = 2\sqrt{Dt} \quad (4)$$

This equation is a fairly good rule of thumb for estimating the extent of diffusion in a given time interval during sintering. When a material diffuses by ~ 0.1μm from the center of a grain boundary to the neck surface, then the approximate annealing time required to have appreciable neck growth must be at least ~ 3 x 10^{-9}/D seconds if *D* is given in units of cm^2/ s. Solidstate diffusivities are generally quite low. Typical values of *D* at sintering, temperatures are 10^{14} 10^{10}, so the annealing times must be on the order of anywhere from 1 minute to 100 hours. Equation (4) also shows that time has a rather weak effect on diffusion. To double the effective diffusion distance, the time must be quadrupled. It is important to realize this fact when trying to determine a firing schedule for the first time [10,11]. If 10% densification occurs after 1 hour at a given temperature, then 20% densification would not be expected until at *least* 4 hours at that temperature, and 40% densification would not occur until at *least* 16 hours at that temperature. In actuality, the driving force for diffusion during sintering decreases continuously as interfacial energy is consumed. Therefore, time is not usually a very effective variable to manipulate during sintering experiments.

UO_2, ThO_2 and PuO_2 can all be sub-stoichiometric as MO_{2-x} with oxygen vacancies being formed as dominant defects, charge compensation being achieved by reducing

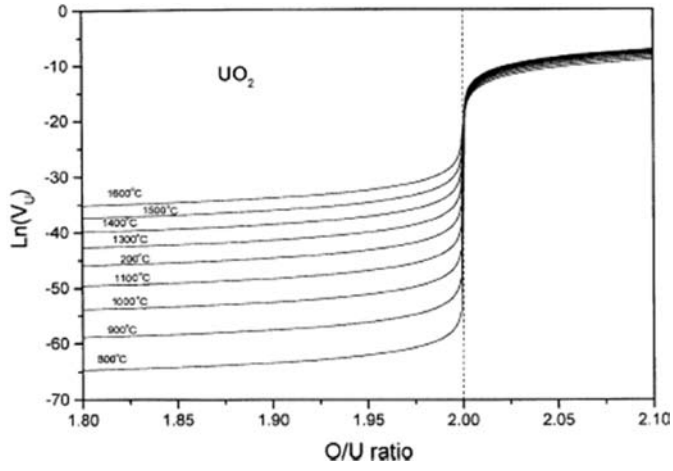

Fig. 1 Concentration of uranium metal vacancies plotted against O/U ratio at various temperatures [13].

Table 1: Standard point defect model of fluorite type oxides $UO_{2\pm x}$ and energies for different defect processes [13].

Defect concentrations:	Stoichiometric $UO_{2.00}$	$[V_U] = 2\exp[-(\Delta G_s - \Delta G_{FO})/kT]$ $[U_i] = 0.5\exp[-(\Delta G_{FU} + \Delta G_{FO} - \Delta G_s)/kT$
	Hyperstoichiometric UO_{2+x}	$[V_U] = x^2\exp[-(\Delta G_s - 2\Delta G_{FO})/kT]$ $[U_i] = (1/x^2)\exp[-(\Delta G_{FU} + 2\Delta G_{FO} - \Delta G_s)/kT$
	Hypostoichiometric UO_{2-x}	$[V_U] = (4/x^2)\exp[-\Delta G_s/kT]$ $[U_i] = (x^2/4)\exp[-(\Delta G_{FU} - \Delta G_s)/kT$
Formation energies, eV	Oxygen Frenkel pair, ΔG_{FO}	3.0
	Metal Frenkel pair, ΔG_{FU}	7.0
	Schottky trio, ΔG_S	6.4
Migration energies, eV	Oxygen vacancy, ΔH^m_{VO}	0.53
	Oxygen interstitial, ΔH^m_{Oi}	0.64
	Metal vacancy, ΔH^m_{VU}	6.0
	Metal interstitial, ΔH^m_{Ui}	8.76

some of the metal atoms, e.g. to Pu^{3+}. UO_2 can also be over stoichiometric as UO_{2+x}, containing oxygen interstitials together with U^{5+} and U^{6+} ions. In fact, UO_{2+x} is the oxide phase showing the largest width of a single-phase extends from $UO_{1.65}$, to $UO_{2.25}$ (at about 2500°C) with a very wide Δ(O/M) of 0.60. Willis [54] has made detailed investigation of the defect structure of UO_{2+x} using Bragg neutron scattering technique. He found the evidence for two types of interstitials, one (O′) displaced from (1/2,1/2,1/2) positions along <110> axis and the other (O″) displaced along the <111> axis. In addition, a significant number of normal oxygen atoms are displaced, thus creating oxygen vacancies which are identical in number with either of the <110> and <111> interstitials. Willis proposed a defect cluster containing two O′ interstitials, two O″ interstitials and two normal oxygen vacancies which is commonly known as 2:2:2 or Willis cluster [10, 11].

Oxygen diffusion

The chemical diffusion of oxygen has the important practical implications such as:

- In fast oxide reactors, this quantity controls the radial redistribution of oxygen in the fuel;
- The kinetics of oxidation of UO_2 to UO_{2+y} or reduction to UO_{2-y} are determined by this property;
- The oxide scale that forms on the Zircaloy cladding exposed to water forms at a rate dependent on D_O in ZrO_2.

The chemical diffusion coefficient in UO_{2+y} describes the flux of oxygen in an O/U gradient. Since the uranium sub-lattice is structurally practically perfect, the gradient is due to a change in the concentration of oxygen interstitials. The U^{5+}/U^{4+} ratio varies in order to maintain electrical neutrality in this gradient of oxygen. For oxidation and reduction, chemical diffusion of oxygen is rate determining. The corresponding diffusion coefficients $\tilde{D}$ are deduced from measurements of the rate at which thermodynamic equilibrium conditions are achieved by diffusion of point within the chemical gradient set-up when the oxygen pressure of the gas atmosphere or the temperature are suddenly changed [1,4].

Uranium Diffusion

There are three types of motion that uranium cations undergo in oxide nuclear fuels. However, they are characterized by the two usual types of diffusion coefficients: self (or tracer) diffusion and chemical (or inter) diffusion. Intrinsic metal atom diffusion is very slow indeed. The most reliable data yield the following Arrhenius equations [8]

$$D^{U,Pu}(UO_2) = 0.65 \exp(-5.6\ eV/kT)\ \ cm^2 s^{-1} \quad (5)$$

$$D^{U,Pu}(ThO_2) = 0.65 \exp(-6.5eV/kT) \quad (6)$$

The plot of 1/T versus log D for UO_2 and ThO_2 is shown in Fig. 2.

Non-stoichiometric Materials

Metal atom diffusion rates depend strongly on deviations from stoichiometry of nuclear ceramic. D_U increases dramatically with x in UO_{2+x} at constant temperature by a factor of ~10^5 between $UO_{2.00}$ and $UO_{2.20}$ at 1500°C. This is predominantly due to an increased concentration of U vacancies in UO_{2+x}. Inter diffusion coefficient D in UO_2-PuO_2 system strongly depends on the oxygen potential, Pu content and temperature [8, 9] as shown in Fig. 3. It is well known that the tracer diffusion coefficient of uranium, D^U and of plutonium, D^{Pu} in UO_{2+x} and MO_{2+x} vary by 4-5 orders of magnitude at constant temperature if the oxygen potential is varied [13]. Diffusion is slow under the reducing condition and it is fast under the oxidizing condition. Typical example is shown in Fig. 4 where densification curves of UO_2-PuO_2 are given. Densification is superior in oxidizing atmosphere like CO_2 indicating diffusion faster in oxidizing atmosphere. The large increase in the diffusion values for hyper-stoichiometric oxide is primarily due to the large metal vacancy concentration in the oxidized state, UO_{2+x} and MO_{2+x} [5, 8, 9]. At constant temperature, the metal defect concentration should depend on x^2. Elaborate work has been carried out by Matzke on MO_{2+x} and has predicted an x^2 dependence for metal self diffusion [2]. The expected strong dependence of D^M on x in MO_{2-x} was also confirmed by experiments on Pu in MO_{2-x} [5]. Three

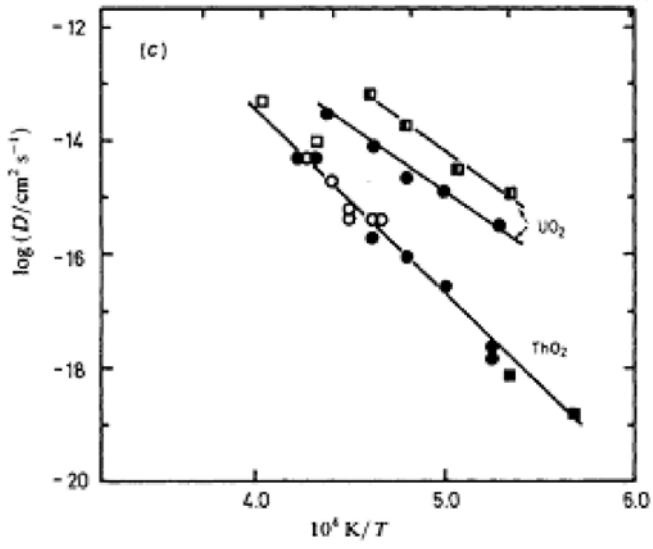

Fig. 2 Arrhenius diagram for metal atom self-diffusion in UO_2 and ThO_2 [5]

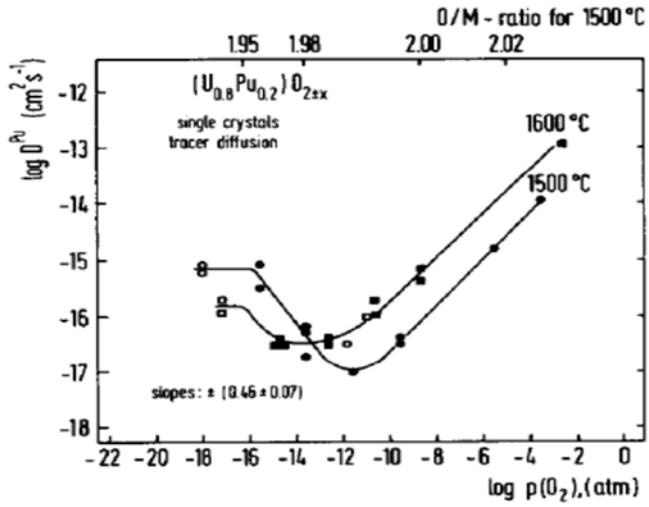

Fig. 3: Dependence of the diffusion of plutonium in $(U_{0.8}Pu_{0.2})O_{2\pm x}$ on oxygen partial pressure at 1500 and 1600°C [8].

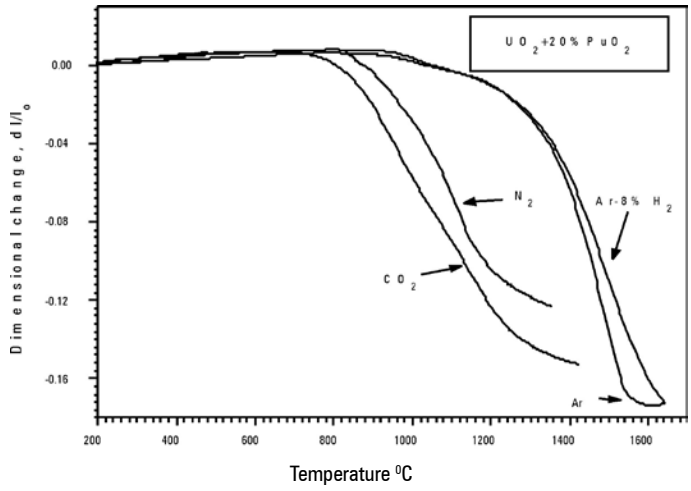

Fig. 4 Densification curves for UO_2-20% PuO_2 in reducing (Ar-8%H_2), inert (Ar) and oxidizing (CO_2) atmospheres [14].

possible mechanisms are suggested for MO_{2-x}, which are listed below [8]:

(a) A vacancy mechanism when O/M > 1.98,

(b) An interstitial mechanism for lower O/M values (1.95 < O/M < 1.98)

(c) A cluster mechanism for O/M < 1.95.

Studies on densification kinetics

For sintering, one of four diffusion paths is usually dominant. The activation energies for each of these diffusion paths are different, and usually the magnitude of the activation energies are ranked in the following order:

1. Lattice diffusion (highest activation energy)
2. Grain boundary diffusion (second highest activation energy)
3. Surface diffusion (third highest)
4. Vapor diffusion (lowest)

The experimental shrinkage curve obtained by dilatometry as shown in Fig. 4, generally follows an equation of the form [15]:

$$\Delta l/l_o = Y = [K(T)t]^n \quad (7)$$

where, 'l_o' is the initial length of the sample at the start of the sintering, 'K(T)' is Arrhenius constant, 't' is the time and 'n' is a constant whose value depends on the sintering mechanism. Many models of sintering have been presented and discussed in the literature [15-20]. A sintering model proposed by Johnson [16,18], in which all the significant mechanisms of materials transport can be identified even though more than one mechanism may be operating simultaneously, has been used in this study. If it is assumed that all the material in the neck comes from grain boundary and if the material transport by surface diffusion, vapor transport are insignificant, then the shrinkage for the first 3.5% can be expressed as [13]:

$$Y^{2.06}\, Y = (2.63\gamma\Omega D_v/kTa^3)Y^{1.03} + (0.7\gamma\Omega bD_b/kTa^4) \quad (8)$$

Where, 'γ' is the surface tension, 'Ω' is the vacancy volume, 'D_v' and 'D_b' are the diffusion coefficients for volume and grain boundary, respectively, 'T' is the temperature, 'a' is the particle radius, 'b' is the thickness of the grain boundary and 'k' is the Boltzmann constant. If only the volume diffusion from grain boundary is operative, then equation (2) becomes [15-18]:

$$Y = (5.34\gamma\Omega D_v/kTa^3)^{0.49}\, t^{0.49} \quad (9)$$

Similarly for grain boundary diffusion

$$Y = (2.14\gamma\Omega bD_b/kTa^4)^{0.33}\, t^{0.33} \quad (10)$$

The equations (9) and (10) predict the slopes of 0.49 and 0.33 in a plot of 'lnY' vs 'ln t' for volume diffusion and grain boundary diffusion, respectively. On differentiating equations (9) and (10) with respect to time, we get,

$$\hat{Y} = 0.49\,(5.34\gamma\Omega D_v/kTa^3)^{0.49}\, t^{-0.51} \quad (11)$$

$$\hat{Y} = 0.33\,(2.14\gamma\Omega bD_b/kTa^4)^{0.33}\, t^{-0.67} \quad (12)$$

The slope of the plot of 'ln$\hat{Y}$' versus 'ln t' will be (n-1) from which the sintering exponent 'n' can be evaluated. From the value of $\hat{Y}$ intercepts, the diffusion coefficient can be evaluated.

The variation of 'log D' with 'T' can be described by an equation of the type:

$$D = D_o \exp(-Q/RT) \quad (13)$$

Where, D_o is the pre-exponential factor and Q is the activation energy.

Results

Some of the typical results obtained for PuO_2 pellets are given below. For this, the shrinkage behavior of the PuO_2 green compacts in the various atmospheres was studied using a push rod type dilatometer. The shrinkage was measured in axial direction. The sample supporter, measuring unit and displaceable furnace of the dilatometer were mounted horizontally. The length change measurements were made by an LVDT transducer, which was maintained at a constant temperature by means of water circulation from a constant temperature bath. The accuracy of the measurement of change in length was within ± 0.1μm. The temperature was measured using a calibrated thermocouple, which is placed directly above the sample. A small force of 0.2 N was applied to the sample through the push rod. The dilatometric experiments were carried out using a flow rate of 18 l/h and a heating rate of 6°C/min. The sintering kinetics has been evaluated for reducing (Ar-8%H_2), inert (Ar) and oxidizing (CO_2 and commercial N_2) atmospheres for the initial stages of sintering. The kinetics has been evaluated in a small temperature range of 1031 to 1092°C for Ar, 1067-1160°C for Ar-8% H_2 and 980-1127°C for CO_2 and N_2 atmospheres. The H_2O/H_2 and CO/CO_2 ratios of the sintering gases (Ar-8%H_2 and CO_2) used in this study were kept smaller than 10^{-4} during this study.

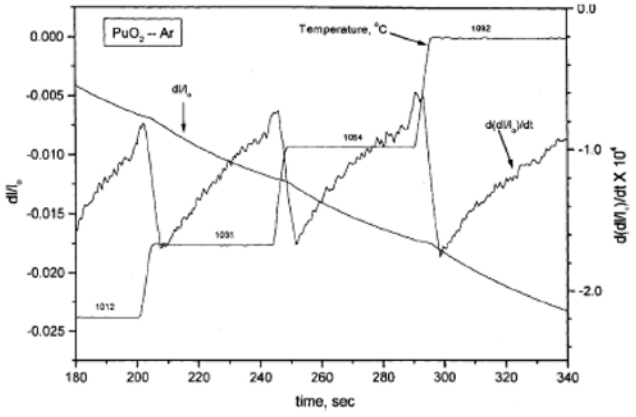

Fig. 5 The variation in shrinkage (dl/lo) and shrinkage rate (dl/dt) occurring in each isothermal step [20].

Fig. 5 shows the time dependent variation of dl/l_o and dl/dt observed in each isothermal step. The parameter 'n' of equation (7) is obtained from the slope of 'log Y' vs 'log t' plot, which is shown in Fig. 6. The value of 'n' obtained for pellets sintered in Ar and Ar-8% H_2 is ~0.50.

Aybers [21] has carried out rate controlled sintering technique on UO_2, $(U,Th)O_2$, $(U,Pu)O_2$ and reported that the mechanism changes with atmosphere used for sintering. He has proposed that the mechanisms during initial stage

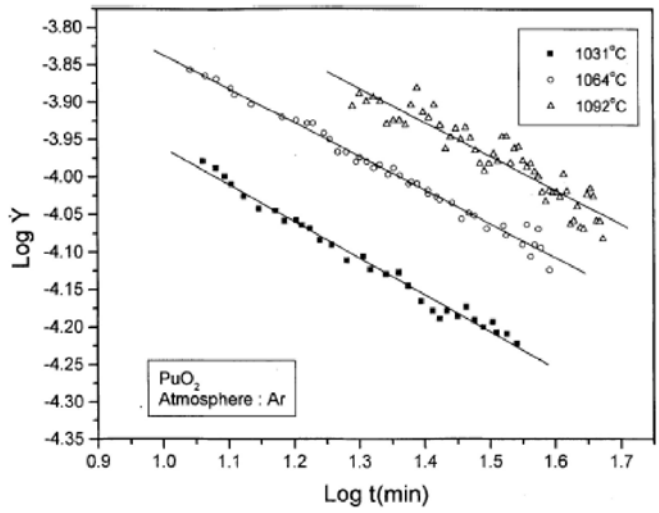

Fig. 6 A plot of log Y vs log t in Ar for different temperatures [20].

of sintering are volume and grain boundary diffusion in reducing and oxidizing atmospheres, respectively. El-Sayed Ali and Sorensen [22] have found n = 0.32 in CO_2 atmosphere for $(U,Pu)O_2$ and n = 0.45 in reducing atmosphere. Our results agree with this observation for reducing atmospheres. The diffusion coefficients are calculated from the intercepts in Fig. 7 and 8 using equation (11) and (12). The 'ln D' vs '1/T' plots for Ar and Ar-8%H_2 atmospheres are given in Figs. 7 and 8, respectively. The activation energies obtained for PuO_2 in Ar and Ar-8%H_2 are 210 and 159 kJ/mol, respectively.

There is no elaborate report available in the literature about the activation energy for PuO_2. The following mechanisms are suggested on the basis of the above mentioned observations:

Cluster mechanism for pellets sintered in Ar-8%H_2 atmosphere and Interstitial mechanism for Ar atmosphere

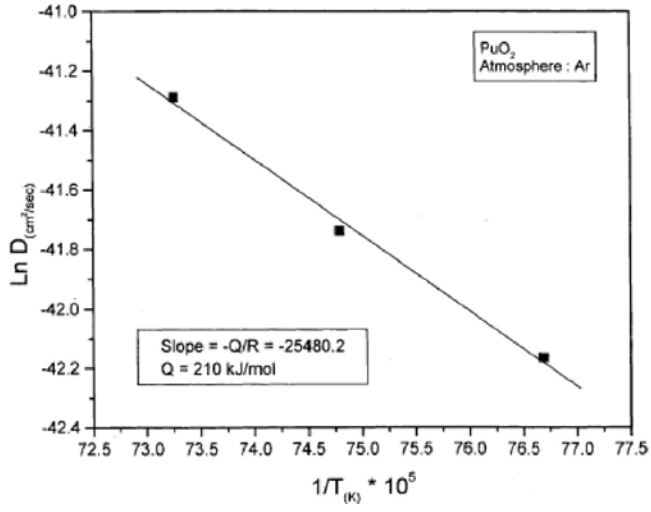

Fig. 7: ln D vs 1/T plots for PuO_2 pellet in Ar atmosphere [20].

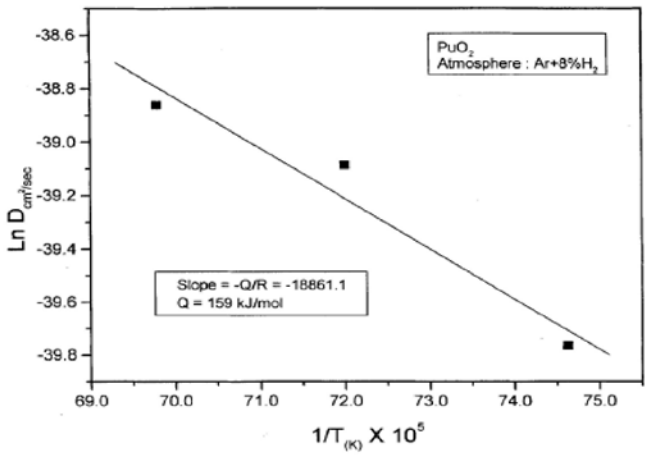

Fig. 8: ln D vs 1/T plots for Ar-8%H_2 atmosphere [20].

Cluster formation is well known to occur in MO_{2-x} at large x values. A few pellets of PuO_2 used for studies were checked for their O/M ratio and was found to be 1.94 for Ar-8%H_2 atmosphere. This clearly indicates that the pellet has considerably deviated from stoichiometry even at ~ 1250°C and hence defects should cluster. The basic unit for such clusters in MO_{2-x} is a nucleus of known sesquioxide Pu_2O_3. The building unit for the clusters are thus of the type Pu^{+3}-V_o- Pu^{+3} where, 'V_o' is the oxygen vacancy. It is reported that clusters of the type Pu^{3+} - V_o - Pu^{3+} is stable even at 1600°C [5]. Schmitz and Marajofsky [19] have given an interesting alternative to interstitial mechanism to explain the increase in D^{Pu} with decreasing O/M ratio. They proposed an interstitial ring mechanism which results in a change of place of U and Pu atoms. This mechanism suggests that two Pu atoms always remain in close proximity to an oxygen vacancy and the migration of U is in the opposite direction to that of the Pu.

Conclusions

Many processes in nuclear ceramics are controlled by diffusion. Although the predominant defects in the fluorite structure are anion defects, the less mobile cation defects that occur at much smaller concentrations, are frequently rate determining for technologically important high temperature mass transport processes such as grain growth, sintering, plastic deformation, creep, etc. Some of the typical examples are shown in this paper. The sintering behavior of PuO_2 was studied in various atmospheres such as inert, reducing and oxidizing atmospheres. It was observed that shrinkage begins at a much lower temperature in oxidizing atmosphere such as CO_2 and commercial N_2. But the shrinkage rate was the highest for Ar atmosphere. The mechanism for the initial stage of sintering was found to be volume diffusion for both oxidizing and reducing atmospheres. The activation energy for sintering was found to be 210 and 159 kJ/mol for Ar and Ar-8%H_2 atmospheres, respectively.

References

1. D.R. Olander, Fundamental Aspects of Nuclear Reactor Fuel Elements, TID-26711-P1, US Department of Energy (1976) 145.
2. Hj. Matzke, Science Of Advanced LMFBR Fuels, Chapter 4, North-Holland, 1986, p. 176.
3. P. Shewmon, Diffusion in Solids, 2nd Ed., The Minerals, Metals & Materials Society (1989).
4. D.R. Olander, *J. Nucl. Mater.*, 389 (2009) 1.
5. Hj. Matzke, in Nonstoichiometric Oxides, ed. T. Sorensen (Academic Press, New York, 1981) p. 156.
6. C.R.A. Catlow, *J. Chem. Soc. Faraday Trans.*, 2 (1987) 1065.
7. D.L. Johnson and T.M. Clarke, *Acta Met.*, 12 (1964) 1173.
8. Hj. Matzke, *J. Chem. Soc. Faraday Trans.*, 86 (1990) 1243.
9. A.B. Lidiard, *J. Nucl. Mater.*, 19 (1966) 106.
10. Hj. Matzke, Atomic Energy Canada Ltd Report AECL - 2585(1966).
11. Hj. Matzke, *J. Phys.*, 34 (1973) 317.
12. T.M. Besmann and T.B. Lindemer, *J. Nucl. Mater.*, 130 (1985) 489.
13. T.R.G. Kutty, P.V. Hegde, K.B. Khan, U. Bask, S.N. Pillai, G.C. Jain, A.K. Sengupta, S. Majumdar, H.S. Kamath and DSC Purushotham, *J. Nucl. Mater.*, 305 (2002) 159.
14. T.R.G. Kutty, P.V.Hegde, K.B. Khan, S. Majumdar and D.S.C. Purushotham, *J. Nucl. Mater.*, 282 (2000) 54.
15. R.L. Coble, *J. Am. Ceram. Soc.*, 41 (1958) 55.
16. D.L. Johnson and I.B. Cutler, *J. Am. Ceram. Soc.*, 46 (1963) 541.
17. W.D. Kingery and M. Berg, *J. Appl. Phys.*, 26 (1955) 1205.
18. D.L. Johnson, *J. Appl. Phys.*, 40 (1969) 192.
19. F. Schmitz and A. Marajofsky, in Thermodynamics of Nuclear Materials 1974,Vol. 1 (IAEA, Vienna, 1975) p. 467.
20. T.R.G. Kutty, K.B. Khan, P.V. Hegde, A.K. Sengupta, S. Majumda and D.S.C. Purushotham, *J. Nucl. Mater.*, 297 (2001) 120.
21. M. Aybers, *J. Nucl. Mater.*, 210 (1994) 73.
22. M. El. Sayed Ali, O.T. Sorensen, *J. Thermal Anal.*, 25 (1982) 175.

Dr T.R.G. Kutty *joined BARC in 1973 after graduating from Kerala University. He subsequently did MSc. (Engg.) and Ph.D. in metallurgy from Indian Institute of Science Bangalore. On obtaining post doctoral fellowship, Dr. Kutty went to McMaster University Hamilton, Canada and worked with Prof. J. D. Embury and Prof. D. S. Wilkinson. He has made significant contributions in the field of nuclear and structural materials. His areas of expertise are: Evaluation of Thermophysical and Thermo mechanical properties including, thermal conductivity, thermal expansion, hot hardness, creep, and fracture toughness of ceramics, densification behaviour, sintering kinetics, structure-property correlation, development of metallic fuels and its properties. He has to his credit a large number of publications. He is a recognized guide Ph. D. Guide of Homi Bhabha National Institute (HBNI).*

A novel pseudo-ion approach in classical MD simulation to determine thermophysical properties of MOX, MC and MN type ceramic nuclear fuels

C. B. Basak
Materials Science Division
Bhabha Atomic Research Centre, Mumbai – 400085.
E-mail: cbbasak@barc.gov.in

Introduction

Molecular dynamics (MD) simulation of nuclear fuels e.g. UO_2, using different classical pair potential models, has been quite successful and numerous studies are being reported in the literatures [1-5]. Also, excellent reviews are available in literature that compares performance of different pair potential models of UO_2 [6]. Classical MD simulation of (U, Pu)O_2 mixed oxide (MOX) has also been attempted by several researchers [7-12]. The so-called transferability problem is the major issue with the potential model employed for the MOX system; i.e. the model provides better description for a specific property of the MOX but fails to do so for any other property for any given potential.

If (U, Pu)O_2 mixed oxide (MOX) is taken as the model system then the usual way to handle such isomorphous system is to fit the potential parameters of UO_2 and PuO_2 system separately. Then in the simulation lattice U ions and Pu ions are distributed "randomly" in their respective lattice points while conserving the intended average composition of the MOX. However, such random distribution may not reproduce the bulk behaviour of the actual system satisfactorily due to the structural degeneracy in the simulated lattice. In other words, there is no guarantee that a particular "random" atomic arrangement of U and Pu atoms would represent the energetic of the true random structure of the MOX. Secondly and more importantly, the uncertainty or error in determining the potential parameters of individual system (i.e. UO_2 and PuO_2 system) would percolate into the MOX system and could affect the results of the simulation in an unpredictable way.

In the present work a new methodology is being proposed where a fictitious or a pseudo ion replaces the random distribution of U and Pu cations. The proposed methodology resembles, in a loose sense, a mean field approach. Such approach solves the structural degeneracy problem; albeit, in an artificial way. Also, in this approach the uncertainty in the fitting of the potential parameter that could affect the simulation results is reduced at least by half. However, the downside of this approach is that specific cation defect energy calculation is not possible; since there is no distinction between different cations. Another issue related to this approach is that for different composition of MOX, the values of the potential parameters should be changed; in contrast to the conventional approach. The very intention of this approach is to get the reliable thermo-physical and thermo-mechanical data of engineering importance under normal as well as in extreme conditions. This approach is quite successful, as will be revealed soon, in predicting the experimentally observed data of $(U_{0.8}Pu_{0.2})O_2$ MOX from ambient temperature to the near melting point.

Classical molecular dynamics

Pseudo-ion approach

The rationale for the pseudo ion approach is primarily based on the fact that isomorphous system can be treated as ideal solid solution; e.g. NaCl-KCl or UO_2-PuO_2 system. The UO_2-PuO_2 system, in particular, could be considered more amenable since the cationic charges are not only the same (i.e. +4) but the cationic masses are also not very different. It could be thus expected that pseudo ion approach may mimic the average dynamics of the actual system; which in turn could reproduce the bulk properties of the material. On the other hand, such approach is not suitable for the calculation of any property that is governed by the local ionic arrangement as stated earlier. Estimation of cation defect energy, for example, may not be accurate while using such pseudo ion approach. Also, the present method may not be suitable where the mass and/or charge of two cations are very different.

In the present case the mass of pseudo ion X is same as that of $(U_{0.8}Pu_{0.2})$ and so also is the charge. Thus, the system $(U_{0.8}Pu_{0.2})O_2$ could be represented as XO_2; where X is the pseudo atom having the same mass as that of $(U_{0.8}Pu_{0.2})$. Considering reactor grade PuO_2, natural UO_2 and MOX composition of 20% PuO_2 the mass of X comes out to be 238.28 a.u. In case of UO_2, a partial ionicity of 60% yields reasonably good results in MD simulation [1-5]. In the present case also 60% ionicity was considered for the XO_2 system. Hence the partial charges Z_X and Z_O come out to be +2.4 and –1.2, respectively. Pictorial representation of pseudo-ion scheme is presented in Fig. 1.

Table. 1. Potential parameters of $(U_{0.8}Pu_{0.2})O_2$ MOX.

Parameters	Unit	O-O pair	X-X pair	X-O pair
a	Å	3.24	3.26	3.53
b	Å	0.330153	0.330153	0.330153
c	eVÅ^{-6}	3.9488	0	0
D	eV	N. A	N. A	0.597914
b	Å^{-1}	N. A	N. A	1.8
*r**	Å	N. A	N. A	2.363
f_0	eVÅ^{-1}	0.042546		

Potential model

In the present study classical pair wise interaction, essentially a Bushing- Ida [13] type of potential model along with Morse type potential, has been chosen. This model is useful while simulating a semi-ionic system. Such combined potential model was first used by Kawamura [14] for studying silicate and other oxide structures and subsequently by Yamada et. al., [1], Basak [3] and Yakub [15] for UO_2. The potential model could be represented in the following form:

$$\varphi_{ij}(r_{ij}) = \frac{z_i z_j e^2}{r_{ij}} + f_0(b_i + b_j)\exp\left(\frac{a_i + a_j - r_{ij}}{b_i + b_j}\right) - \frac{c_i c_j}{r_{ij}^6} + D_{ij}\left[\exp\{-2\beta_{ij}(r_{ij} - r_{ij}^*)\} - 2\exp\{-\beta_{ij}(r_{ij} - r_{ij}^*)\}\right] \quad (1)$$

The first term is the long range Coulomb interactions while the second term accounts for core repulsion and the third one is due to van der waals weak attraction. The last one is the Morse type potential and is applicable only for anion-cation pair and r_{ij}^* is the anion-cation bond length.

Fitting of potential parameters

The free parameter of the fitting is given by the following equation [16]:

$$F = \sum_i \omega_i (\Lambda_e^i - \Lambda_c^i)^2 \quad (2)$$

where Λ^i is the i^{th} observable of the system and ω_i is the weighing factor for that particular observable. Subscripts *e* and *c* denotes the expected (i.e. known from experiments) and calculated values (i.e. from simulation). For an ideal fitting the value of *F* should be equal to zero.

Keeping the Coulombic terms untouched, attempt was made to fit the other parameters. In order to get the initial approximation of $b_O + b_X$ (i.e. $b_{X\text{-}O}$) the following formula was applied [17]. Though this relation is more appropriate to determine the ρ_{ij} value used in Buckingham type potential, but as an initial guess the following equation works fine.

$$b_i + b_j = \frac{1.85}{\sqrt{I_i} + \sqrt{I_j}} \quad (3)$$

where, I_i and I_j are the first ionization potential values (in eV) for *i* and *j* species respectively. Consequently, initial guess value of $b_{X\text{-}O}$ comes out to be 0.300869 Å; considering I_O=13.61eV and I_X=6.05eV (same as I_U). An initial guess for the '*a*' values of oxygen ion pair ($a_{O\text{-}O}$) and cation ion pair ($a_{X\text{-}X}$) were twice their corresponding ionic radii; for O^{2-} and X^{4+} (U^{4+}) ionic radii were taken as 1.14 Å and 1.26 Å respectively. The van der Waals weak interaction for cations was neglected. Initial values of rest of the parameters were taken from our earlier study [3].

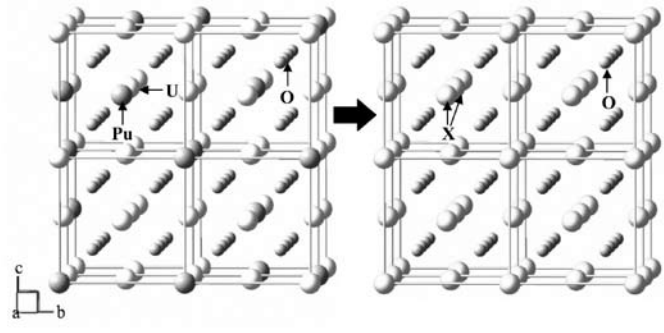

Fig.1. Pictorial depiction of pseudo-ion scheme where randomly distributed individual U and Pu ions in the lattice were replaced by a pseudo-ion X having adjusted atomic weight.

Four-point method was adopted to improve the fitting of potential parameters. Details of such limited point fitting have been described elsewhere [17]. The lattice parameter values at 300K, 800K, 1300K and 1800K were taken from the Martin's data [18]. Eventually the free parameter, from equation (2), can be expressed as:

$$F = \sum_T \left[a_e(T) - a_c(T)\right]^2 \quad (4)$$

where *a* is the lattice parameter and the sum was taken over the above mentioned four temperatures. The weighing factor for each parameter was kept as unity. The potential parameters thus obtained are given in Table 1.

Set up, conditions and simulation techniques

Both UO_2 and PuO_2 hold stable fluorite structure (CaF_2 type) and each unit cell contains four U^{4+} (or Pu^{4+}) ions and eight O^{2-} ions. In the present study the MD supercell was constructed with an array of 10×10×10 unit cells in three

mutually orthogonal direction with 4000 cations ($X^{+2.4}$) and 8000 anions ($O^{-1.2}$).

The initial random velocity was chosen from the Maxwell-Boltzmann distribution at 298K. The equation of motion was integrated using Beeman's algorithm, which is of predictor-corrector type, with the unit time step (Δt) of 1.0×10^{-15}s. Both constant pressure-temperature (NPT) and constant volume-temperature (NVT) simulation was performed using Nosé -Hoover thermostat to control the temperature. Before accumulation of the thermodynamic data, equilibrium run of 2×10^4 time steps were made at desired temperature and pressure. During the NPT simulation Parrinello-Rahman constant stress method [19] was applied in order to judge the structural reproducibility of the system ensuring the required pressure control.

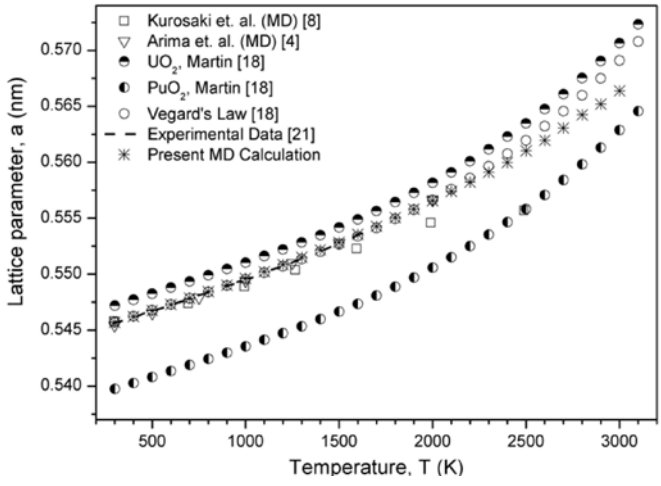

Fig.2. Lattice parameter of $(U_{0.8}Pu_{0.2})O_2$ MOX as a function of temperature; lattice parameter of UO_2 and PuO_2 are also shown here for Vegard's law calculation and comparison.

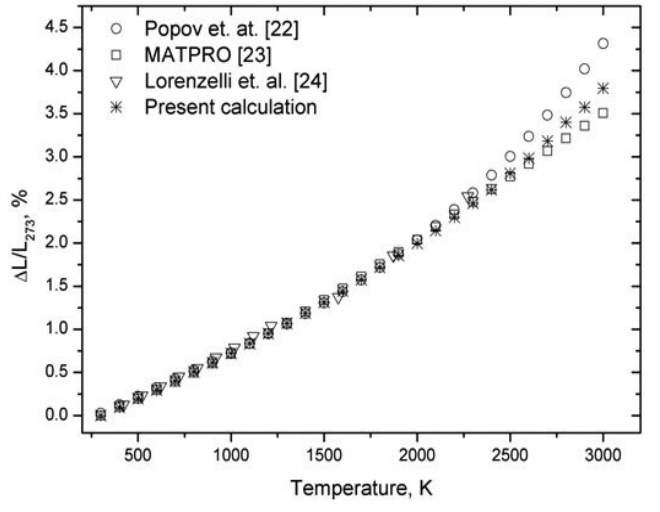

Fig.3. Thermal expansion of $(U_{0.8}Pu_{0.2})O_2$ MOX as a function of temperature

The calculation was performed with the classical molecular dynamics code MOLDY [20]. To ensure effective coupling between system and external pressure bath; the extended system mass parameter was adjusted at each temperature. It ensures better pressure and temperature control of the simulated system.

Results and discussions

Lattice parameter

Lattice parameters obtained by Vegard's law using Martin's data [18], Kurosaki's data [8], Arima's data [9] and experimental data of TPRC [21] together with the calculated lattice parameter, as a function of temperature, are presented in Fig. 2. The calculated results show only a nominal monotonous deviation from the experimental values beyond 2400K. The calculated lattice parameters can be fitted with a polynomial function of temperature as follows:

$$a_{20\%MOX} = 544.159 + 4.87\times10^{-3}\,T + 6.197\times10^{-7}\,T^2 - 8.187\times10^{-11}\,T^3 + 5.272\times10^{-14}\,T^4 \quad (5)$$

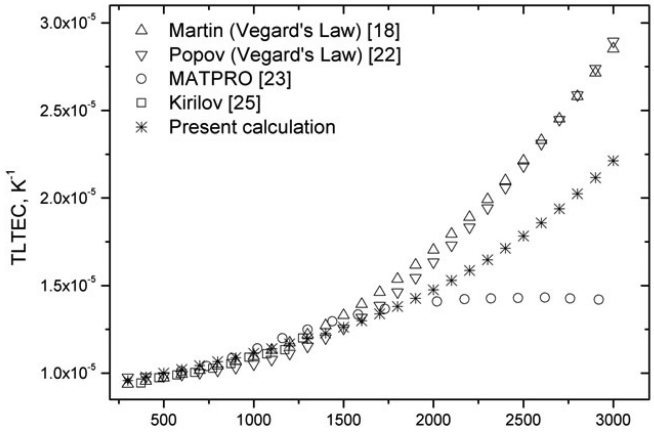

Fig.4. True linear thermal expansion coefficient (TLTEC) of $(U_{0.8}Pu_{0.2})O_2$ MOX as a function of temperature.

where, *a* is in pm and *T* in K. It should also be noted that Martin's data [18] used in Fig. 2 are based on Vegard's law derivation from the experimental data of UO_2 and PuO_2 match well with the calculated lattice parameter values up to about 2200K. The calculated results also match quite well with the experimental data [21] and Arima's data[9]. However, at higher temperature (T> 2200K) the graph trend moves toward PuO_2 side suggesting deviation from the ideal-solution behaviour.

Thermal expansion

Relative linear thermal expansion, $\Delta L/L_{273}$ for $(U_{0.8}Pu_{0.2})O_2$ compared with the experimental data [22] are presented in Fig. 3; along with the data of MATPRO [23] and

Lorenzelli [24]. It could be seen from the figure that almost upto 2300K all data match well with the calculated data. However, beyond 2300K the calculated data are in between the Popov's data [22] and MATPRO data [23]. Derivation of relative linear thermal expansion in MATPRO uses the following equation:

$$\varepsilon(\%) = K_1 T - K_2 + K_3 \exp\left(\frac{E_D}{k_\beta T}\right) \quad (6)$$

where, K_1, K_2, K_3 and E_D are constants; for UO_2 and PuO_2 these values are given in Table 2. Finally, using these data one can employ the Vegard's law as follows:

$$F_{(U_x Pu_{1-x} O_2)} = x.F_{UO_2} + (1-x).F_{PuO_2} \quad (7)$$

Table. 2. Values of constants used for calculation of relative linear thermal expansion [23].

Constants	Unit	UO_2	PuO_2
K_1	K^{-1}	1.0×10^{-3}	9.0×10^{-4}
K_2	…	0.3	0.27
K_3	…	4	7
E_D	J	6.9×10^{-20}	7.0×10^{-20}

where, F is the physical property in concern and x is mol fraction of UO_2.

True linear thermal expansion coefficient (TLTEC) was calculated from 300K to 3000K and can be expressed as follows:

$$\alpha(T) = \frac{1}{L_{273}}\left(\frac{dL}{dT}\right)_P \quad (8)$$

where, L could be either unit cell length or the MD cell length. The variation in TLTEC with temperature is shown in Fig. 4; along with the data from Martin [18], Popov [22], MATPRO [23] and the Kirilov [25]. All data matches reasonably well up to 1600K and then the calculated data tend to deviate from the Popov's data and Martin's data. It is to be noted that both Popov and Martin's data are based on Vegard's law derivation (using Eq. 7) and hence the present results indicate the deviation from ideality. Since, TLTEC uses temperature derivative of lattice parameter; hence deviation from ideality is more realistic for the TLTEC than the values of lattice parameter alone. So, it seems likely that deviation from ideality should be taken as 1600K (and not 2200K derived from Fig. 2). It is interesting to see that the calculated TLTEC values lie between Vegard's law data [20, 22] and the MATPRO data [23].

Isothermal compressibility

The isothermal compressibility can be expressed as follows:

$$\beta_T = -\frac{1}{V}\left(\frac{dV}{dP}\right)_T \quad (9)$$

where, V and P stands for volume (lattice) and pressure, respectively. Lattice volume was calculated with varying pressure from 0.1 MPa to 1.5 GPa with an interval of 100 MPa at all the temperature from 300K to 3000K. The compressibility values fit well to the standard exponential relationship [17]:

$$\beta_T = \beta_0 \exp\left[aT + bT^2\right] \quad (10)$$

where, β_0 is the isothermal compressibility at absolute zero temperature; inverse of which is the isothermal bulk modulus at 0K and its fitted value was found to be 198.5 GPa; as shown in Fig. 5. It is to be noted that Yamada's and Kurosaki's MD result (i.e. isothermal compressibility) [1, 8], based on the model of randomly replaced ions in lattice, show extreme jump beyond 2200K. It is a known fact that there exists Bredig transition in UO_2 beyond 2200K [1-5] due to the instability in oxygen sub-lattice. However, unstable oxygen sub-lattice does not guarantee a drastic rise in isothermal compressibility in UO_2; since cation sub-lattice remains stable and also there is no drastic change in lattice parameter over the temperature. Thus, such drastic change of isothermal compressibility, as reflected in Yamada's and Kurosaki's results, manifests the shortfall of the randomly substituted lattice-site model. Present calculation clearly show well behaved curve for isothermal compressibility of MOX, though, this system too shows Bredig transition as will be discussed in next section.

Specific heat (C_p)

C_p can be thought of as summation of C_V and the heat capacity terms for dilatation, electronic excitation etc. Excepting the dilatation term (often called C_d) all other terms are usually quite smaller than the C_V value and hence can be ignored safely. C_V can readily be calculated using classical MD under NVT condition; and eventually C_P can be expressed as follows:

$$C_P = C_V + \frac{\gamma V_m T}{\beta_T} \quad (11)$$

where, γ is the volume expansion coefficient, V_m is the molar volume, β_T is the isothermal compressibility and T is the absolute temperature. All these parameters can readily be determined from the MD simulation. The variation of C_P as a function of T is presented in Fig. 6; along with

the C_P values found in literatures [1, 8, 25- 28]. Also, the C_P data of 20%MOX is provided using Neumann-Kopp's rule. The present C_P values match reasonably well to the reported data.

The inset graph in Fig. 6 shows a clear peak having onset at around 2400K indicating a second order transition; similar observation was made by Potashnikov et. al. [11] and they inferred a Bredig transition around that temperature. In the present case also Bredig transition could be observed and will be discussed separately in the next section.

Bredig transition

The inherent high temperature instability of the oxygen sub-lattice in fluorite-type structure is often termed as Bredig transition [29]. Bredig transition is a second order transition often characterized by the sudden rise in the anionic diffusivity (the so-called super-ionic conductivity) or from the enthalpy data.

MD simulations carried out by several researchers have already been proved the presence of a second order Bredig transition between 2500K- 2670K for UO_2 [1-5]. The onset of Bredig transition is usually taken as 0.8-0.84 T_m, where T_m is the melting temperature at absolute scale [30, 31]. 20%PuO_2 MOX is expected to have a lower melting point (than UO_2) due to the addition of low-melting PuO_2 in UO_2. Moreover, UO_2 and PuO_2 being isomorphous it could be expected that 20%MOX should also exhibit similar second order transition, albeit at a lower temperature. The mean-squared displacement data obtained from the simulation result were used to derive the ionic diffusivity using Einstein's relationship as follows:

$$D_i = \underset{t\to\infty}{Lt}\frac{1}{6t}\left\langle \left| r_i(t) - r_i(0) \right|^2 \right\rangle \qquad (12)$$

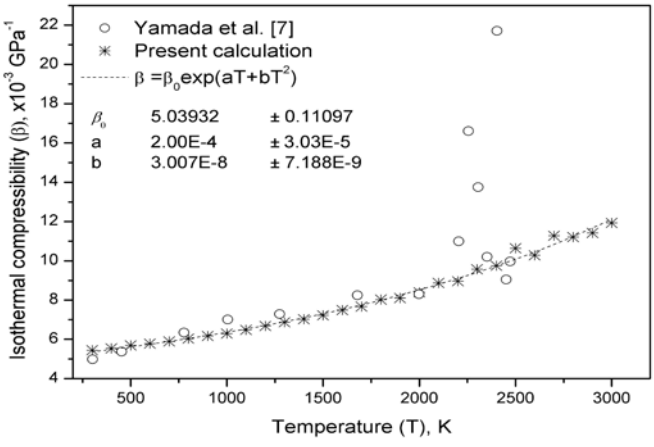

Fig.5. Isothermal compressibility of $(U_{0.8}Pu_{0.2})O_2$ MOX as a function of temperature.

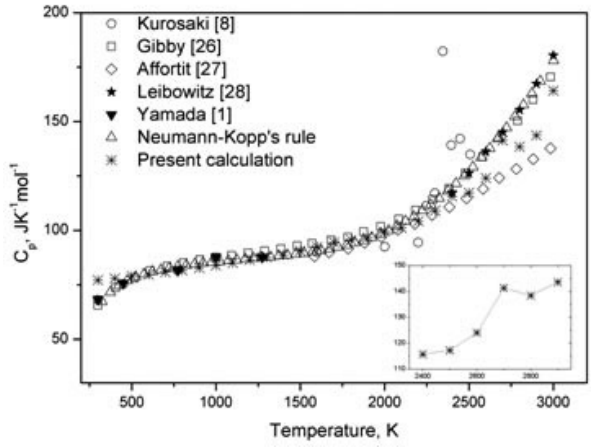

Fig.6. Specific heat (C_p) of $(U_{0.8}Pu_{0.2})O_2$ MOX as a function of temperature.

Where, D_i is the diffusivity of the ionic species *i* and *t* is the time. The result presented in Fig. 7 clearly shows the oxygen super-ionic conduction that starts at around 2400K. It is evident from the result that 20%PuO_2 MOX has lower Bredig transition temperature than that of UO_2 as predicted from their melting point. Such accurate prediction of physical phenomenon clearly demonstrates the supremacy of the pseudo-ion approach over the randomly substitute model; which shows massive scatter of data near the Bredig transition in MOX making it difficult to calculate the Bredig transition temperature accurately [7-8].

It is important to note that the sudden rise in diffusivity of oxygen ion is only the manifestation of the Bredig transition. Oxygen sub-lattice instability, at higher temperature, due to unbalanced inter-atomic force is the root cause for this second order transition. In fact if one deploys Arrhenius equation to plot ln(D) vs. 1/T, as shown in Fig. 8, it can be seen that the oxygen diffusion mechanism is different before and after the Bredig transition. The dashed line shown in Fig. 8 corresponds

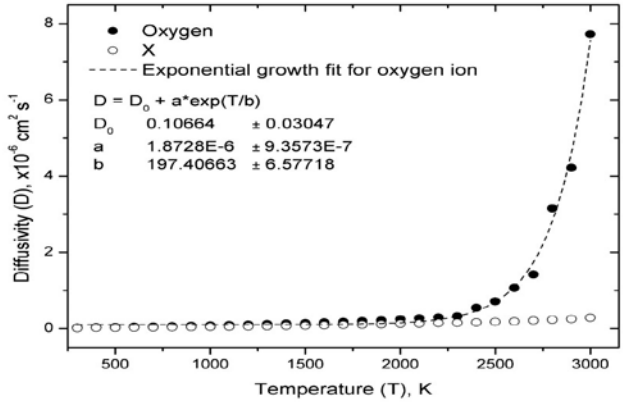

Fig.7. Self-diffusivity of pseudo-ion (X) and oxygen ion in $(U_{0.8}Pu_{0.2})O_2$ MOX as a function of temperature; showing Bredig transition at around 2400K.

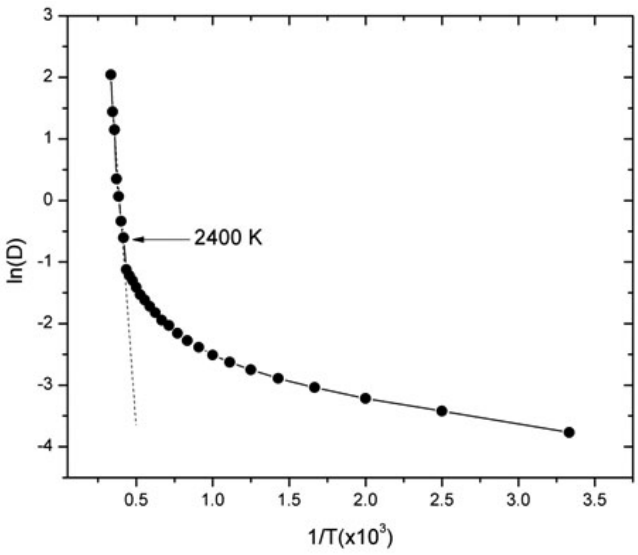

Fig.8. Arrhenius plot of oxygen ion. The linear region beyond Bredig transition is marked as dashed line

to the high temperature part of the Arrhenius plot after Bredig transition.

Future scope of pseudo-ion potential

As discussed in section 2.1, potential parameters derived from pseudo-ion scheme are not generic across the composition. However, there exists possibility to determine the inter atomic potential parameters from the two terminal compounds. In the case of UO_2-PuO_2 MOX, if one knows potential parameters for pure UO_2 and pure PuO_2 it is in principle possible to find out the potential parameter of any MOX of given composition using pseudo-ion approach [32]. But such extrapolation of the parameters would be highly non-linear and some parameter may be invariant. It is, therefore, a very interesting and unexplored field worth further investigation.

On the other hand, it is clear that such pseudo-ion classical MD approach can also be applicable for other fuel systems; e.g. UC-70%PuC (Mark-I fuel for FBTR), UC-55%PuC (present Mark-II fuel for FBTR), UO2-28%PuO2 (peripheral fuel composition for PFBR), ThO_2 based MOX (for AHWR fuel) could be potential candidates for psedo-ion MD simulation to evaluate important thermophysical properties of practical interest.

Conclusions

A new pseudo-ion approach in classical pair potential has been proposed here in context of classical molecular dynamics simulation. The main idea is that any ionic system $(A_mB_n)C$ could be represented as XC, where X is the pseudo-ion having the same mass as that of (A_mB_n); provided the masses are nearly the same and the charges are identical. This approach is successfully implemented using classical molecular dynamics simulation of $(U_{0.8}Pu_{0.2})O_2$ in the temperature range of 300-3000 K. The calculated lattice parameter and linear thermal expansion are in a good agreement with known experimental data. The isothermal compressibility was calculated with varying pressure from 0.1 MPa to 1.5 GPa with an interval of 100 MPa at all the temperature from 300K to 3000K. It shows an exponential behavior like for UO_2 system. The specific heat (C_P) was calculated as a function of T using isothermal compressibility and compared with known MD results and experimental data. Calculated mean-squared displacement clearly shows that there exists Bredig transition that takes place at about 2400 K; at slightly lower temperature than that for UO_2.

References

1. K. Yamada, K. Kurosaki, M. Uno, S. Yamanaka, *J. Alloys Comp.*, 307 (2000) 1.
2. N. D. Morelona, D. Ghaleba, J. M. Delayea, L. Van Brutzela, *Phil. Mag.*, 83 (2003) 1533.
3. C. B. Basak, A. K. Sengupta, H. S. Kamath, *J. Alloys and Comp.*, 360 (2003) 210.
4. T. Arima, S. Yamasaki, Y. Inagaki, K. Idemitsu, *J. Alloys Comp.*, 400 (2005) 43.
5. E. Yakub, C. Ronchi, D. Staicu, *J. Nucl. Mater.*, 389 (2009) 119.
6. K. Govers, S. Lemehov, M. Hou, M. Verwerft, *J. Nucl. Mat.*, 376 (2008) 66.
7. K. Yamada, K. Kurosaki, M. Uno, S. Yamanaka, *J. Alloys Comp.*, 307 (2000) 1-.
8. K. Kurosaki, K. Yamada, M. Uno, S. Yamanaka, K. Yamamoto, T. Namekawa, *J. Nucl. Mater.*, 294 (2001) 160.
9. T. Arima, S. Yamasaki, Y. Inagaki, K. Idemitsu, *J. Alloys Comp.*, 415 (2006) 43.
10. S.I. Potashnikov, A.S. Boyarchenkov, K.A. Nekrasov, A.Ya. Kupryazhkin, *ISJAEE,* 8 (2007) 43.
11. S.I. Potashnikov, A.S. Boyarchenkov, K.A. Nekrasov, A.Ya. Kupryazhkin, *J. Nucl. Mater.*, 419 (2011) 217.
12. P. Tiwary, Axel van de Walle, B. Jeon, N. Grønbech-Jensen, *Phys. Rev. B,* 83 (2011) 094104.
13. Y. Ida, *Phys. Earth. Planet. Inter.*, 13 (1976) 97.
14. K. Kawamura, *Springer Series in Solid-State Sciences,* 103 (1992) 88.
15. E. Yakub, C. Ronchi, D. Staicu, *J. Chem. Phys.*, 127 (2007) 094508.
16. A. R. Oganov, J. P. Brodholt, G. D. Price, *Phys. Earth. Planet. Inter.*, 122 (2000) 277.
17. C. B. Basak, *Comp. Mat. Science,* 40 (2007) 562.
18. D. G. Martin, *J. Nucl. Mater.*, 152 (1988) 94.
19. M. Parrinello, A. Rahman, *J. App. Phys.*, 52 (1981) 7182.
20. K. Refson, MOLDY: User's Manual, htttp://www.earth.ox.ac.uk/~keith/moldy/html (1988-2000)

21. Thermophysical Properties of Matter, The TPRC Data Series Vol.5. IFI/Plenum Data, New York (1970)
22. S.G.C. Popov, J.J. Ivanov, V.K. Yoder, Oak Ridge National Laboratory, Thermophysical properties of MOX and UO2 Fuels Including the Effects of Irradiation, ***ORNL/TM-2000/351 (2000)***
23. SCDAP/RELAP5/MOD3.2 Code Manual, Vol. IV:MATPRO – A, Library of Materials Properties for Light-Water Reactor Accident analysis, NUREG/CR-6150, (INEL-96/0422), Rev. 1, Oct. (1997)
24. R. Lorenzelli, M. El Sayed Ali, *J. Nucl. Mater.,* 68 (1977) 100.
25. P. L. Kirillov, Thermophysical Properties of Materials for Nuclear Power Engineering: Recommended Practice. − Obninsk: Edition OIATE, 1994 (Russian)
26. R. L. Gibby, L. Leibowitz, J.F. Kerrisk, D.G. Clifton, *J. Nucl. Mater.,* 50 (1974) 155.
27. C. Affortit, J. Marcon, *Revue Internationale des Hautes Temperatures et des Refractaires,* 7 (1970) 236.
28. L. Leibowitz D. F. Fischer M. G. Chasanov, "Enthalpy of Molten Uranium--Plutonium Oxides" ANL -8082 (1974)
29. M .A. Bredig, *Colloq. Int. CNRS.,* 205 (1972) 183.
30. P. Browning, G.J. Hyland, J. Ralph, *High. Temp.–High. Press.,* 15 (1983) 169.
31. J. Ralph, *J. Chem. Soc. Faraday Trans.,* 2 (1987) 83.
32. C. B. Basak, A. S. Kolokol, *J. Am. Ceram. Soc.,* 95 (2012) 1435.

Dr. C. B. Basak *got his B. E. Degree in 1999 from Bengal Engg. College, Shibpore (WB) in Metallurgical Engineering, securing the first position. For this he got Indranil Award from Indian Institute of Mineral, Mining and Metallurgy. He then joined IISc, Bangalore for M. Tech. securing 5th rank in GATE-2000. However, he left IISc and joined 44th batch of OCES. After successful completion of the orientation course he joined Radiometallurgy Division, BARC in 2001; and is presently working in Materials Science Division. He received his doctoral degree from Indian Institute of Technology, Bombay in 2010 for his experimental physical metallurgical work on U-Zr alloys. His work on classical molecular dynamics simulation in nuclear fuels is well recognized internationally. Especially for his proposed potential parameters of UO_2, which is now referred as Basak Potential of UO_2 in international journals, he has received felicitation from ICTP in 2010 and Young Enggineer Award 2010 from Department of Atomic Energy. His field of interests encompasses classical MD, DFT and phonon based energetics calculations as well as experimental phase transformation studies.*

Thermal Expansion Studies on Candidate Ceramic and Glass-ceramic Matrices for Nuclear Waste Immobilization

R. Asuvathraman, R. Raja Madhavan, Hrudananda Jena, Kitheri Joseph and K.V. Govindan Kutty
Liquid Metals and Structural Chemistry Division,
Indira Gandhi Centre for Atomic Research, Kalpakkam - 603 102, India.
E-mail: kvg@igcar.gov.in

Abstract

The thermophysical properties such as thermal expansion are key parameters determining the long-term performance and chemical durability of radioactive waste forms meant for nuclear waste disposal. Large magnitudes of the thermal expansion coefficient can lead to thermal shock and consequent material cracking and degradation in the temperature gradient between the centre and surface of the radioactive waste form. This paper discusses the results of thermal expansion measurements on waste forms synthesized in the laboratory using simulated waste compositions expected from the reprocessing of fast reactor fuels. Single-phase monazite and multi-phasic synroc were selected as typical ceramic hosts for the high-level waste from the PUREX process, and glass-bonded sodalite and glass-bonded apatite were chosen as glass-ceramic matrices for the waste from pyrometallurgical reprocessing. Thermal expansion measurements were carried out by high-temperature X-Ray powder diffractometry as well as by bulk dilatometry.

Introduction

Safe sequestration of the highly radioactive nuclear waste in durable matrices is an important activity in the back end of the nuclear fuel cycle. In the closed fuel cycle, reprocessing of the spent nuclear fuel is carried out either by the aqueous PUREX process or by a pyrometallurgical non-aqueous process such as electrorefining in a molten salt medium. For the first generation high-level waste from the former (a nitric acid solution of intense radioactivity), borosilicate glass has been accepted as a suitable matrix almost worldwide [1, 2]; however, crystalline ceramic matrices are fast emerging as a superior alternative [1-3]. For the immobilization of the radioactive elements left behind after electrorefining in the molten LiCl-KCl salt bath, a zeolite based glass-ceramic, viz., glass bonded sodalite, has been demonstrated by U.S. researchers [4, 5]; other composites such as glass-bonded apatite are also under investigation [6-10]. It is therefore, imperative to develop methods for the viable synthesis of these materials and study their physico-chemical properties so that they can be developed as radioactive waste forms on an industrial scale.

Among the various crystalline ceramics under consideration for immobilization of radioactive waste, synroc is the most widely characterized material. It is an assemblage of four mutually compatible titanate phases, viz., zirconolite ($CaZrTi_2O_7$), hollandite ($BaAl_2Ti_6O_{16}$), pervoskite ($CaTiO_3$) and rutile (TiO_2) [11,12]. These phases are capable of incorporating almost all the constituents of the radioactive waste as dilute solid solution, as determined by their ionic radii and chemical valence. Synroc is considered to be an ideal host for HLW from fast reactor as these wastes contains large amounts of noble metals and actinides. Monazite, a mixed rare earth orthophosphate, is a natural mineral known to exist for billions of years [13]. It possesses excellent chemical and radiation stability despite the high α-decay dose from the thorium and uranium contained in it [14-16]. The advantage of monazite (e.g., $CePO_4$) as the host is that it is a single-phase ceramic and can accommodate all the elements of the radwaste as solid solution in its unique crystal structure. It is particularly suitable for the rare earth and traces of actinide elements expected from the reprocessing of fast reactor fuels. A typical pyrometallurgical waste will be in the chloride form, and would mainly comprise the alkali, alkaline earth and rare earth fission products. Neither glass nor common ceramics can incorporate halide in the structure to any significant extent; however, some aluminosilicate and apatite ceramics do take up halides in their structure, e.g., sodalite and chlorapatite. Both these are natural minerals of considerable chemical durability. Sodalite has the formula $Na_8Al_6Si_6O_{24}Cl_2$, and apatite can be represented as $M_{10}(PO_4)_6X_2$, where (M= Ca, Sr, Ba; X = OH, Cl, F) [6-8,17]. Their resistance to leaching by ground water can be strengthened further by providing an additional barrier by bonding the ceramic with a durable glass such as borosilicate glass, thus yielding a glass-ceramic composite.

The integrity and long term performance of a radioactive waste form are determined to a significant extent by its thermophysical properties, viz., thermal expansion coefficient, thermal conductivity and heat

capacity [1]. The presence of the heat generating nuclides in the waste can considerably raise the temperature of the waste form. If the thermal conductivity of the matrix is low, large thermal gradients will be developed between the bulk and the outer surface of the waste body. If the matrix also has high thermal expansivity, it can cause severe thermal shock to the waste form, leading to its cracking up and a consequent increase in surface area. This is an undesirable scenario, as it may result in increased leaching of the radioactive elements by ground waters.

Experimental

Synroc samples were synthesized by a wet chemical method employing a nanoanatase reagent as the source for titanium oxide. Slurry was prepared by dispersing the titanium dioxide reagent in nitric acid to which stoichiometric amounts of the other reactants, namely, aluminium nitrate, zirconyl nitrate, barium carbonate and calcium carbonate were added. The simulated waste (15 wt.% loading, Table 1) solution was prepared separately by dissolving the various constituents as soluble salts, elements or oxides in nitric acid. The waste solution was gradually added to the reactant slurry with constant stirring. It was heated to dryness at 423 K, and the dried powder was calcined at 1023 K for 3 h in Ar/4% H_2. The calcined powders were consolidated by hot uniaxial pressing (HUP) into dense cylinders of 10 mm diameter and 10 mm length. The monazite, $CePO_4$, was prepared by a solution chemistry route by mixing solutions of AR grade $Ce(NO_3)_3 \cdot 6H_2O$ and $NH_4H_2PO_4$ in stoichiometric quantities. It was dried and then heated to 573 K for 4 h. Sintering of the pellets was done at 1473 K for 10 h. The density of the pellet was 91% TD. The $CePO_4$ with 10 wt.% simulated waste (composition in Table 1) from FBTR fuel of 150 GWd/t burn-up and one year cooling was prepared in a similar way. Glass-bonded sodalite was fabricated by a three-step process: first incorporating the simulated chloride waste salt into dehydrated zeolite 4A by high temperature equilibration at 850 K, followed by blending the salt loaded zeolite with a boroaluminosilicate glass, and finally sintering at high temperature and pressure to yield the glass-ceramic. The (simplified) simulated waste salt composition is given in Table 2. Cylindrical samples of 10 mm diameter and 10 mm length were prepared by HUP at 973K. The apatites $M_{10}(PO_4)_6Cl_2$ (M=Ca,Sr, Ba) and simulated waste loaded apatite with borosilicate glass bonding were prepared by solid state reaction at 1023K by using the waste composition in Table 2, and stoichiometric amounts of the reactants $M(OH)_2$, $NH_4H_2PO_4$, NH_4Cl and a borosilicate glass.

Table 1. Simulated PUREX waste composition

HLW Oxide	Wt.%	HLW Oxide	Wt.%
Ag_2O	0.73	TiO_2	0.10
BaO	3.75	NiO	0.77
CdO	0.33	Fe_2O_3	2.78
Ce_2O_3	6.27	Eu_2O_3 (Eu+Am)	1.54
Cs_2O	10.41	Gd_2O_3 (Gd+Pm+Np+Cm)	0.84
Cr_2O_3	0.38	Nd_2O_3	9.66
La_2O_3	3.42	PdO	6.86
MoO_3 (Mo+Tc)	14.73	Pr_6O_{11}	3.45
MnO_2	0.15	Rh_2O_3	2.99
Rb_2O	0.49	RuO_2	9.97
SnO_2	0.41	Sm_2O_3	2.73
SrO	1.19	TeO_2	1.38
ZrO_2	8.49	Y_2O_3	0.73
U_3O_8 (U+Pu)	5.47		
Total		100.00	

Linear thermal expansion of a crystalline phase was studied using powder samples in the temperature range of 298 to a maximum of 1173 K by high-temperature XRD employing a Philips X'pert Pro MPD system in a vacuum of about 10^{-5} torr. Platinum powder mixed with the sample was used as internal standard for temperature calibration. Lattice parameters at various temperatures were calculated using the X'pert Plus version 1.0 software (Philips, Netherlands). From the measured lattice parameters, thermal expansion data were derived. The details of the experimental method are given elsewhere [18]. Thermal expansion of bulk solids was measured by using a well calibrated push-rod dilatometer built in-house [19], in air at a heating rate of 2 K/min. The samples were in the form of dense cylinders of 10 mm diameter and 10 mm height.

Table 2. Simulated pyrometallurgical waste composition

	LiCl-KCl	$NdCl_3$	$BaCl_2$	CsCl
Wt. %	87	9	2	2

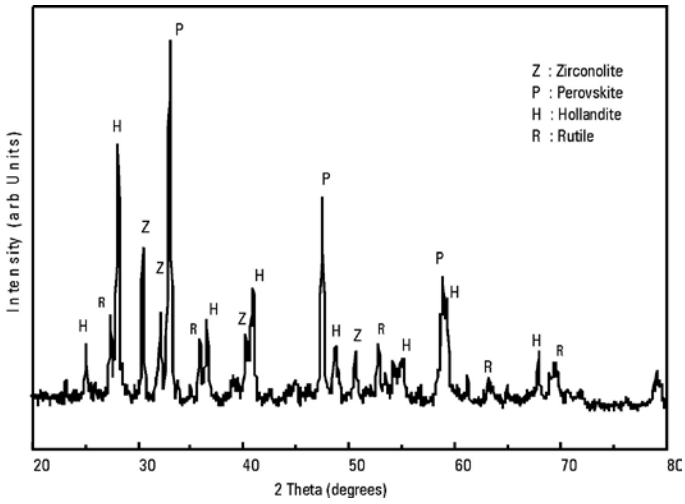

Fig. 1. X-Ray diffractogram of the simulated waste loaded synroc.

Results & Discussion

Fig. 1 shows the XRD pattern of the synroc sample and Fig. 2 shows the dilatometric trace depicting the variation of % bulk thermal expansion with temperature for the monoliths with and without incorporated waste: synroc-C containing 15 wt.% simulated waste and synroc-B, respectively. The expansion behavior of the two materials can be seen to be nearly the same, which indicates that the incorporation of the waste elements in the different phases does not alter the overall thermal expansivity of the phase assemblage. The average linear expansion coefficient in the temperature range of measurement works out to approximately 10×10^{-6} K^{-1}, a value typical of common ceramics.

Fig. 3 displays the XRD patterns of a pristine monazite phase ($CePO_4$) and monazite with 10 wt.% simulated high-level waste (HLW) incorporated in the structure. The monazite phase is retained in the simulated waste form, and no other phase is detected by XRD. Dilatometric measurements are more appropriate to study the expansion characteristics of multiphase composites such as synroc. High temperature X-Ray powder diffractometry (HTXRD) is a powerful tool in delineating the thermal expansion of a specific phase in multiphase assemblages, or the axial expansion behavior of low-symmetry crystal systems. In the present investigation, the thermal expansion behavior of $CePO_4$ and $CePO_4$ with 10 wt% simulated HLW were measured by using both HTXRD and dilatometry.

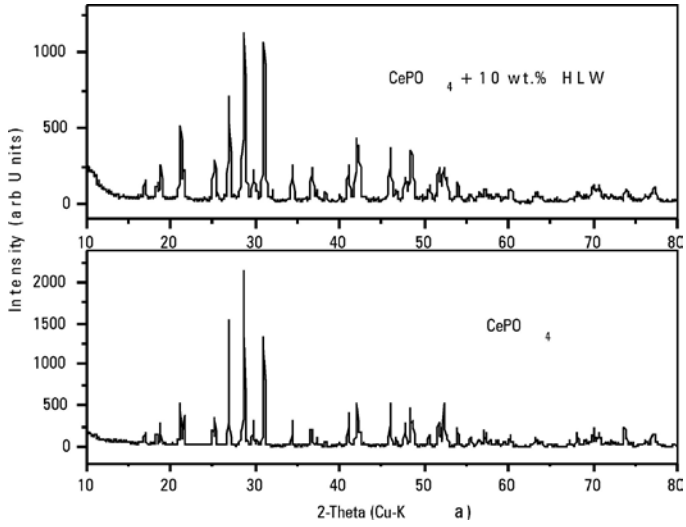

Fig. 3. XRD patterns of the $CePO_4$ and $CePO_4$ with 10 wt.% simulated waste sintered at 1473 K.

In order to compare the results from the two different techniques, it is assumed that one third of the volume expansion gives the average linear thermal expansion,

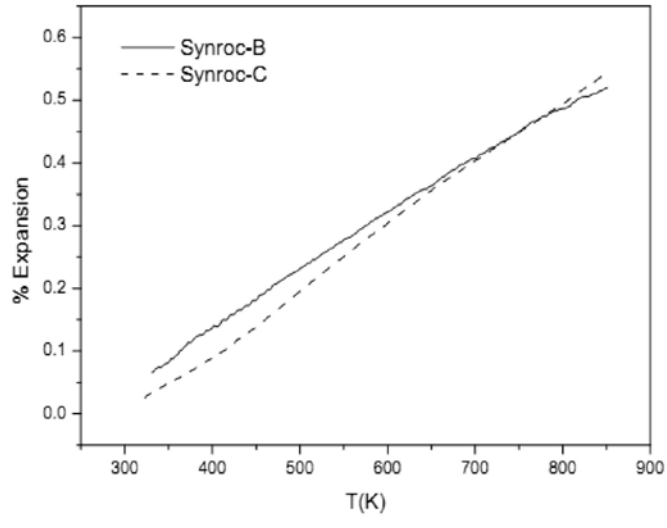

Fig. 2. Bulk thermal expansion of synroc-B and synroc-C monoliths.

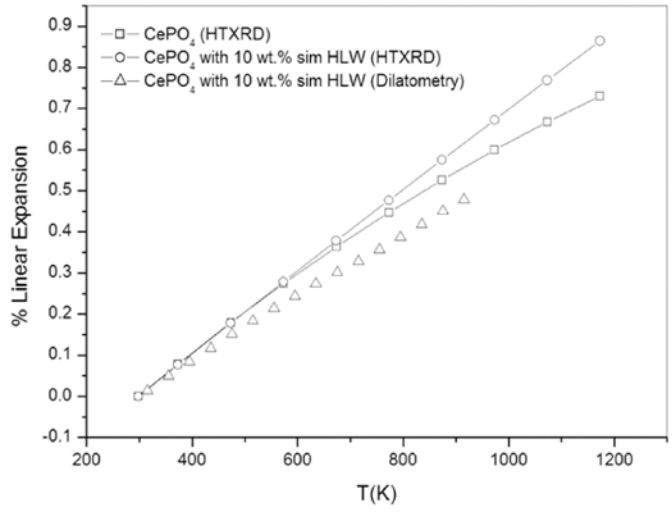

Fig. 4. Linear thermal expansion of $CePO_4$ and $CePO_4$ with 10 wt% simulated waste.

and is plotted in Fig. 4. The monoclinic lattice parameters were calculated at different temperatures and the variation of unit cell volume with temperature evaluated. It can be inferred from Fig. 4 that the thermal expansion behavior of $CePO_4$ monazite is not significantly altered by waste loading. At 900 K, the thermal expansion measured by the two methods for the samples vary from 0.45 to 0.6%. The deviation seen may be due to differences in specimen characteristics and the method of measurement in the two techniques; the unit cell expansion is monitored in HTXRD, whereas the length of the bulk sample is probed in dilatometry.

In glass bonded sodalite (GBS), apart from the glass, the phase assemblage consists of sodalite as the major crystalline phase, with traces of nepheline (Fig. 5). Linear thermal expansion of the cubic sodalite phase was studied in the temperature range of 298-1173 K by high-temperature XRD. Lattice parameters at various temperatures were calculated systematically. The sodalite phase in GBS has a cubic structure, and the lattice parameter (a) varies smoothly with temperature (Fig. 6). A least-squares fit gives the equation: $a = 8.85858 - 3.36622 \times 10^{-5} T + 1.38488 \times 10^{-7} T^2$. Fig. 6 also compares the lattice parameter of the sodalite phase of the present study with the data on pure sodium-sodalite reported by Hassan et al. [20]. Although the variation of lattice parameter with temperature is similar, the absolute values are different because the sodalite sample studied by Hassan et al. is the pure sodium form of sodalite, whereas the sodalite phase of the present waste form is expected to contain at least a portion of the fission products (Cs, Ba and Nd) along with Li, K, and Na.

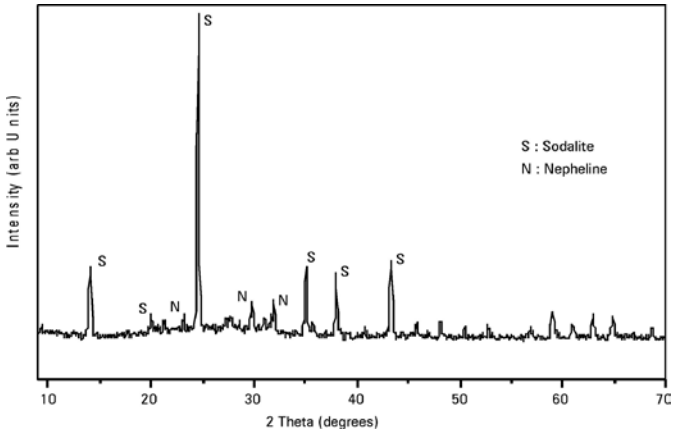

Fig. 5. X-Ray diffractogram of simulated glass bonded sodalite.

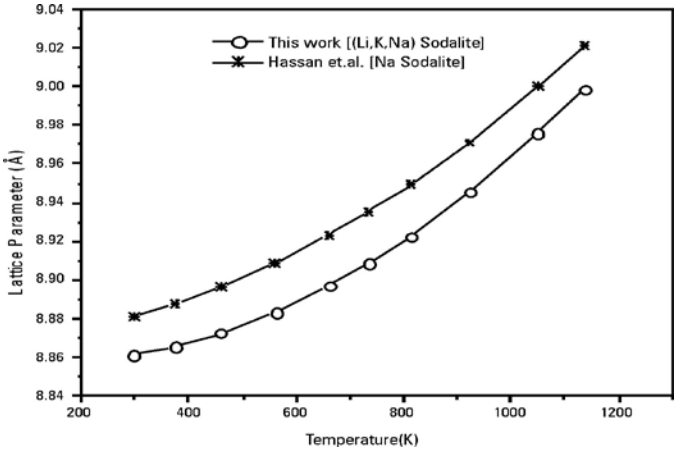

Fig. 6. Variation of sodalite lattice parameter with temperature.

The percentage thermal expansion and coefficient of average linear thermal expansion at 1135 K for the sodalite phase were found to be 1.55% (Fig. 7) and 18.6×10^{-6} K^{-1} respectively. Fig. 7 also shows that the thermal expansion behavior of the present sodalite phase is almost the same as that of pure sodalite.

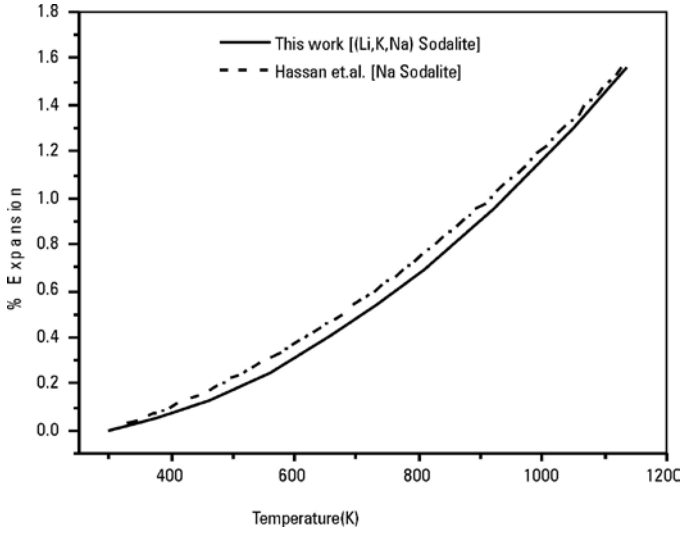

Fig.7. Lattice expansion of sodalite as a function of temperature.

The bulk thermal expansion of the GBS measured by dilatometry is shown in Fig. 8. The change in slope observed at 795 K is due to the glass transition of the glass phase; this provides a reliable value of the glass transition temperature of the residual glass phase coexisting with the ceramic phase. The thermal expansion of the glass-ceramic at 795 K is found to be about 0.6%, and the corresponding expansion coefficient is 12.8×10^{-6} K^{-1}. These studies have demonstrated that the GBS waste form has good thermal stability and incorporation of the waste constituents does not alter the expansion behavior of the sodalite phase to any significant extent.

Fig. 9 shows the formation of the single-phase apatites $M_{10}(PO_4)_6Cl_2$ (M = Ca, Sr and Ba). The waste

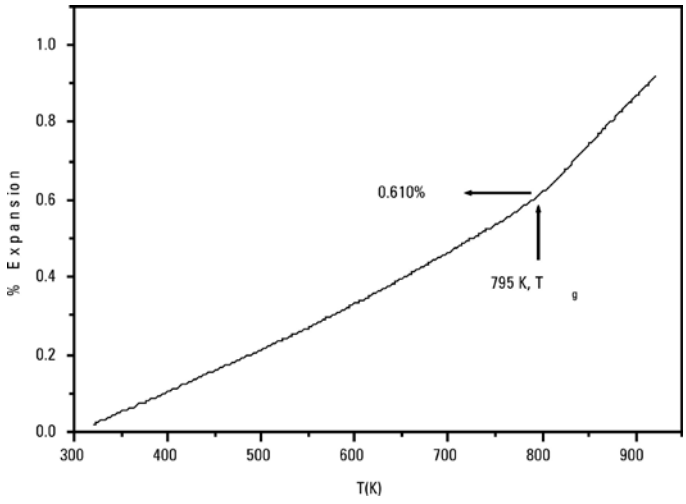

Fig 8. Bulk expansion of simulated glass bonded sodalite.

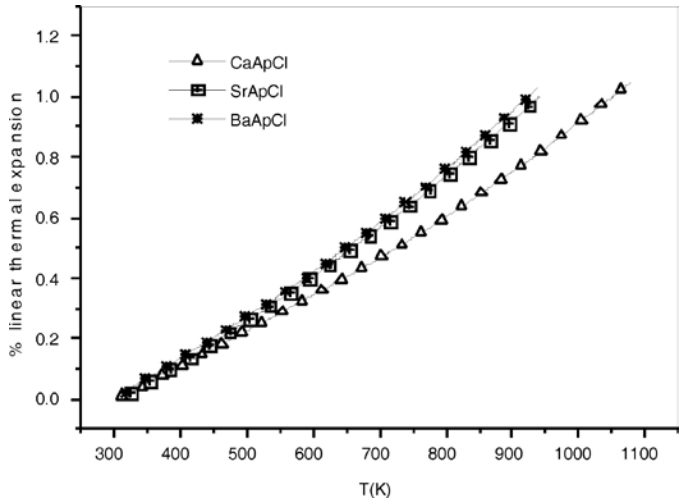

Fig. 10. Linear thermal expansion of $M_{10}(PO_4)_6Cl_2$ (M = Ca, Sr, Ba).

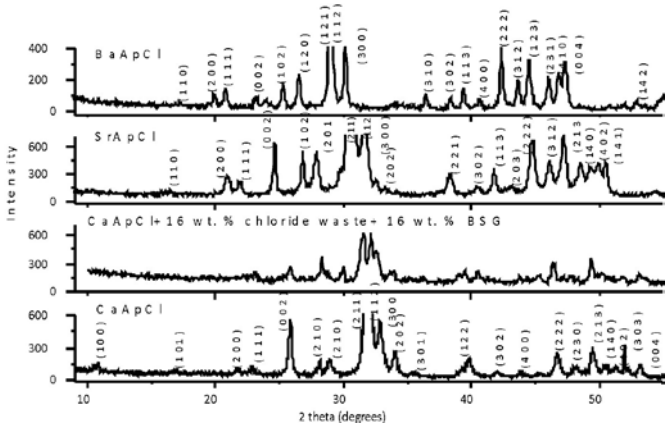

Fig. 9. XRD patterns of $M_{10}(PO_4)_6Cl_2$ (M=Ca,Sr,Ba) and glass-bonded CaApCl-composites.

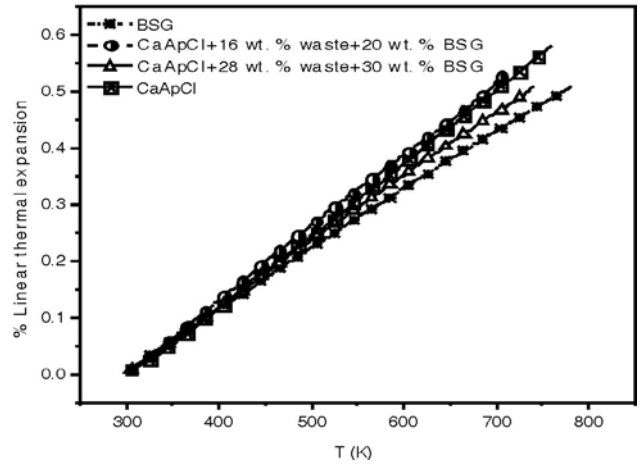

Fig.11. Linear thermal expansion of CaApCl, BSG and simulated CaApCl glass-ceramics.

loaded glass-ceramics based on them also showed only the crystalline chlorapatite phases (e.g., Fig. 9). The bulk thermal expansion of the chlorapatite phases is shown in Fig. 10. Thermal expansion of the calcium compound is the lowest among the three alkaline earth chloroapatites. The average coefficient of thermal expansion of the chlorapatites of calcium (CaApCl), strontium (SrApCl) and barium (BaApCl) are found to be 12.79×10^{-6} K^{-1}, 15.79×10^{-6} K^{-1} and 16.29×10^{-6} K^{-1}, respectively in the temperature range of 298 - 940 K. The increasing thermal expansivity with the increase in the alkaline earth ionic radius can be ascribed to the decreasing ionic interaction in the solid.

The calcium chlorapatite glass-ceramic with 16 wt. % waste loading showed nearly the same bulk thermal expansion as the pristine chlorapatite ceramic phase (Fig. 11). The waste loaded glass-ceramics showed higher thermal expansion compared to the pristine borosilicate glass (BSG) phase employed for the fabrication of the glass-ceramic, and the expansion can be seen to come down when the glass content in the composite is increased.

The observed behaviour can be attributed to the chemical interaction among constituent elements of the matrix.

From a survey of the above results, it can be seen that the materials are quite promising systems for the immobilization of radioactive waste. They can be synthesized and consolidated to high-density bodies by common methods. Their thermal expansion behavior is quite typical of technical ceramics. All can be classified as high-expansion materials since their thermal expansion coefficient is higher than 8×10^{-6} K^{-1} [21]. However, they can be expected to be compatible with the canister materials such as stainless steels. The waste loading may have to be adjusted suitably in order to guard against the occurrence of steep temperature gradients in the radioactive waste form and any consequent thermal shock to the monolith.

References

1. Radioactive Waste Forms for the Future, Eds. W. Lutze and R.C. Ewing, Elsevier Science Publishers B.V. (1988).
2. I.W. Donald, Waste immobilization in Glass and Ceramic Based Hosts: Radioactive, Toxic and Hazardous Wastes, John Wiely & Sons (2010).
3. I.W. Donald, B.L. Metcalfe, R.N. Taylor, J. Mat. Sci., 32, (1997) 5851.
4. L.J. Simpson and D. J. Wronkiewicz, in: W. Gray and K. Knecht (Eds.) Scientific Basis for Nuclear Waste Management XX, 465 (1997) 441.
5. M.A. Lewis, D.F. Fischer and L. J. Smith, J. Am. Ceram. Soc., 76 (11) (1993) 2826.
6. P.Trocellier, Ann. Chim. Sci. Mater., 25(2000) 321.
7. R.Bros, J.Carpena, V.Sere and A.Beltritti, Proc. Migration 95 , Radiochim. Acta, 74 (1996) 277.
8. I.W. Donald, B.L. Metcalfe, S.K. Fong, L.A. Gerrard ,D.M. Strachan, R.D. Scheele, J. Nucl. Mater., 361 (2007) 78.
9. H.Jena, B.K.Maji, R.Asuvathraman, K.V.G. Kutty, J. Non-Cryst. Solids, 358 (2012) 1681.
10. S. Priebe, Idaho National Laboratory, 2007, INL/CON-07-12580
11. R.C. Ewing and W. Lutze, Ceramics International, 17 (1991) 287.
12. A. E. Ringwood, S. E. Kesson, N. G. Ware,W. Hibberson and A. Major, Nature, 278 (1979) 219.
13. O.H. Leonardos Jr., Econ. Geol., 69 (1974) 1126.
14. L.A. Boatner and B.C. Sales, Radioactive waste forms for the future, Eds. W. Lutze and R.C. Ewing, Elsevier Science Publishers B.V. (1988) 495.
15. L.A. Boatner, G.W. Beall, M.M. Abraham, C.B. Finch. P.G. Huray and M. Rappaz, Scintific basis for nuclear waste management, Vol. 2, Ed. C.J.M. Northrup Jr, Plenum Press, Boston (1979) 289.
16. G.J. McCarthy, W.B. White and D.E. Pfoertsch, Mater. Res. Bull., 13 (1978) 1239.
17. E.Fleet, Y.Pan, J. Solid State Chem., 112 (1994) 78.
18. K.V. Govindan Kutty and R. Asuvathraman, ITAS Bulletin, 1 (2005) 5.
19. K.V. Govindan Kutty, R. Asuvathraman, M.V. Krishnaiah, V. Ganesan, R. Parthasarathy, D. Sai Subalakshmi, B. Suhasini, K.C. Srinivas, K.A Gopal and P.V. Kumar, IGCAR, Report IGC-283, 2006.
20. I. Hassan, S. M. Antao and J. B. Parise, American Mineralogist, 89 (2004) 359.
21. D.K. Agrawal, C.-Y. Huang and H.A. McKinstry, International J. Thermophys., 12 (1991) 697.

R. Asuvathraman *obtained his M.Sc. degree in Chemistry from University of Madras and M.Sc.(Engg.) degree in Metallurgy from Indian Institute of Science, Bangalore. He graduated from the 29th Batch of the BARC Training School and joined IGCAR in 1986. He has been working in the area of materials characterization using high temperature x-ray diffraction. His research interests are x-ray Rietveld analysis, novel synthesis of materials, and ceramic matrices for radioactive waste immobilization and thermophysical properties of materials.*

R. Asuvathraman *obtained his M.Sc. degree in Chemistry from University of Madras and M.Sc.(Engg.) degree in Metallurgy from Indian Institute of Science, Bangalore. He graduated from the 29th Batch of the BARC Training School and joined IGCAR in 1986. He has been working in the area of materials characterization using high temperature x-ray diffraction. His research interests are x-ray Rietveld analysis, novel synthesis of materials, and ceramic matrices for radioactive waste immobilization and thermophysical properties of materials.*

Dr. Hrudananda Jena *joined BARC Training School in 1990 (34th batch) after his post graduation (M.Sc,Chemistry) from Utkal University,Odisha. He joined IGCAR in 1991. Subsequently obtained Ph.D in Materials Science from Indian Institute of Science, Bangalore (2005). He did post doctoral studies on materials for energy producing devices sponsored by US-DOE in Southern University, USA. Currently, he is working on development of matrices for radwaste immobilization and their property measurements. His research interests are X-ray crystallography and understanding structure property correlation of ceramics and glass-ceramics. He has nearly 60 publications in various international journals and conference proceedings. He is life member of Society for Materials Chemistry, SAEST and SACSE.*

Kitheri Joseph *obtained her M. Sc degree in Chemistry in 1989 from Loyola College, Chennai. She joined Department of Atomic Energy through 33rd batch of the BARC training school and joined Indira Gandhi Centre for Atomic Research, Kalpakkam in 1990. Her current interest includes studies on synthesis and thermophysical properties of matrices needed for the immobilization of nuclear waste.*

Dr. K.V. Govindan Kutty *took his M.Sc. and Ph.D degrees in Chemistry from Indian Institute of Technology, Madras. He graduated from the 21st Batch of the BARC Training School, and joined Indira Gandhi Centre for Atomic Research, Kalpakka in 1978. His research interests are novel synthesis of materials, ceramic and glass matrices for radioactive waste immobilization, x-ray methods of analysis, and thermophysical properties of materials. He heads the Materials Chemistry Division, and is also a Professor of the Homi Bhabha National Institute.*

Structural and thermal expansion behavior of thoria-based fuels

A. K. Tyagi
Chemistry Division
Bhabha Atomic Research Centre
Mumbai - 400 085, India.
E-mail: aktyagi@barc.gov.in

Abstract

Thorium has attracted considerable attention in the recent past as it is expected to play an important role in the third stage of the Indian nuclear power generation program due to a vast abundance of thorium in India. Thermal expansion behavior is an important property, which governs the integrity of a nuclear fuel. This article intends to provide an overview of thermal expansion studies on thoria-based systems, which have relevance to Advanced Heavy Water Reactors (AHWR).

Thoria-based fuels for Advanced Heavy Water Reactors: A brief introduction

Thorium has attracted lots of attention in the recent past as it is expected to play an important role in the third stage of the Indian nuclear power generation program [1,2] due to a vast abundance of thorium in India. Thorium is also three times more abundant than uranium in earth's crust. ThO_2 is bestowed with excellent properties like low thermal expansion, high melting point, high thermal conductivity (compared to UO_2), higher neutron absorption coefficient, high chemical and radiation stability. These properties make ThO_2 an ideal choice as a host lattice for futuristic nuclear reactors. The Advanced Heavy Water Reactors (AHWRs) are being contemplated to play a key role in thorium utilization. Since thorium itself is not a fissile material in the thermal region of neutrons, it is proposed to use about 2 to 6% of fissile uranium and plutonium dioxides in the ThO_2 matrix. Thermal expansion is an important thermo-physical property, which directly affects the performance of a fuel. However, unlike the urania-based fuels, the thoria-based fuels are not well investigated and in view of this requirement, a research program on the investigation of thermal expansion behavior of thoria-based mixed oxide systems have been initiated in our group [3-15]. One of the major activities is on the bulk and lattice thermal expansion behavior of different thoria-based systems relevant to the proposed thorium oxide based nuclear reactors. In addition to various thoria-based virgin fuels, we have also investigated several ternary compounds of thoria with some of the fission products.

Techniques for investigating thermal expansion of solids

Thermal expansion can be classified as bulk thermal expansion or lattice thermal expansion. The bulk thermal expansion can be measured by a thermo-dilatometer whereas one needs an X-Ray diffractometer with a high temperature attachment (HT-XRD) for measurement of lattice thermal expansion. In case of dilatometry, one needs a rod shape pellet preferably with high bulk density. A push rod, in contact with the sample, is used to transmit the dilation in sample to a transducer, which is commonly a linear variable differential transformer (LVDT) or a dial gauge. One can perform dilatometry experiments either in static air or a flowing atmosphere or vacuum, depending upon the experimental requirement. It is not possible to get anisotropic thermal expansion by dilatometry, unless the sample is in the form of a big single crystal. The bulk thermal expansion coefficient is thus presented as (a_l) and defined as

$$\alpha_l = \frac{l_T - l_o}{l_o(T - T_o)} \quad (1)$$

Where, l_T = length of the materials at the temperature T

l_o = reference length i.e. length of material at reference temperature T_o.

a_l = coefficient of thermal expansion in $^oC^{-1}$ or K^{-1}.

In high temperature XRD, as its name suggests, XRD pattern of a powder sample is recorded at different temperatures and indexed or refined to get the cell parameters and in turn one gets the lattice thermal expansion. It may be added here that the dilatometry and HT-XRD in conjunction are very versatile tools for studying various microscopic phenomenon like point defects, etc. A comparison of dilatometry and high temperature XRD for thermal expansion studies is given in Table I.

The average volume thermal expansion of a materials is defined in terms of the volumes at initial and final temperatures and thus given as

$$\alpha_v = \frac{V_T - V_o}{V_o(T - T_o)} \quad (2)$$

Where, V_T = Unit cell volume of the materials at the temperature T

V_o = reference volume i.e., volume of material at reference temperature T_o.

Table I: Merits and demerits of High Temperature XRD and Dilatometry

Dilatometry	High Temperature XRD
Only bulk thermal expansion can be investigated	Lattice and volume thermal expansion can be investigated
Anisotropic thermal expansion cannot be investigated	Anisotropic thermal expansion can be investigated
Usually large amount of sample is required (~ 2-5 g)	Small amount of powder sample is sufficient (100 mg)
High bulk density pellets are preferred	There is no such requirement
Any solid material can be investigated	Only crystalline solids can be investigated
Sensitivity is good (~mm)	Sensitivity is very good (~ Å)
Sinterability studies can be performed	Sinterability studies cannot be performed
Only first order phase transition can be investigated	All types of phase transitions can be investigated
It does not give any information on origin of thermal expansion	It gives information on crystallographic origin of thermal expansion behavior

Preparation and characterization of the samples

Most of the thorium based-mixed oxides were prepared by a multi-stages heating protocol so as to ensure better homogeneity. Appropriate mixtures were pressed into 8 mm pellets and heated at 1473 K for 36 hours, followed by another heating after regrinding at 1573 K for 36 hours. Each product was once again ground well, pelletized and heated at 1673 K for 48 hours followed by slow-cooling to room temperature at the rate of 2 K/min. in static air. The XRD patterns were recorded by X-Ray diffractometry (Philips Model PW 1710) with monochromated Cu-Kα radiation. In order to determine the solubility limits, the lattice parameters were refined by a least-squares method. In order to study the lattice thermal expansion behavior of these samples, High temperature X-Ray powder diffraction (HT-XRD) studies were carried out using a Philips Xpert Pro Unit having an Anton Paar high temperature attachment. The XRD patterns were recorded at different temperatures under vacuum of the order of 10^{-5} torr. The lattice thermal expansion behavior of these mixed oxides was investigated by refining the cell parameters at different temperatures using least-squares methods.

Results and discussion

Lattice thermal expansion studies in ThO_2-UO_2 system

As mentioned earlier, thorium itself is not a fissile material in the thermal region of neutrons and hence in order to utilize the large resource of thorium, it is proposed to use about 2 to 6 wt. % of uranium and plutonium dioxides in the ThO_2 matrix. It was found that all the reports in literature are on thermal expansion of ThO_2 containing higher amounts of UO_2 i.e., ≥ 10 %. There were no reports of ThO_2 containing 2-6 wt. % UO_2 which is the composition of one component of the fuel for Advanced Heavy Water Reactor. Therefore, lattice thermal expansion of several compositions ThO_2-2, 4 and 6 wt. % UO_2 were studied by High temperature X-Ray powder diffraction. The XRD patterns were recorded in the range $10^o < 2\theta < 90^o$ from room temperature to 1623 K. All the XRD data were recorded in a dynamic vacuum of the order of 2×10^{-5} torr. The observed cubic lattice parameters at room temperature for ThO_2 and ThO_2-2 wt. % UO_2, ThO_2-4 wt. % UO_2, ThO_2-6 wt. % UO_2 were 5.599(1), 5.591(1), 5.589 (1), 5.585(1) Å, respectively. The systematic decrease in lattice parameter, which can be explained based on the relative ionic size considerations, indicates the homogeneous incorporation of U^{4+} into the lattice of ThO_2. Typical XRD patterns of one of the samples, i.e., ThO_2 - 4 wt. % UO_2, at different temperatures are given in Fig.1. In order to study the thermal expansion behavior, the unit cell parameters were determined, as a function of temperature. The coefficients of average lattice thermal expansion (α_a) of ThO_2 and ThO_2 - 2, 4 and 6 wt. % of UO_2 are 9.67×10^{-6}, 9.82×10^{-6}, 10.09×10^{-6} to 10.37×10^{-6} K^{-1}, respectively. It can be seen that there is a systematic increase in the average thermal expansion coefficient after incorporating UO_2 into ThO_2. This trend can be correlated to the higher melting point of ThO_2 as compared to that of UO_2. In general higher the melting temperature, lower is the thermal expansion coefficient [16].

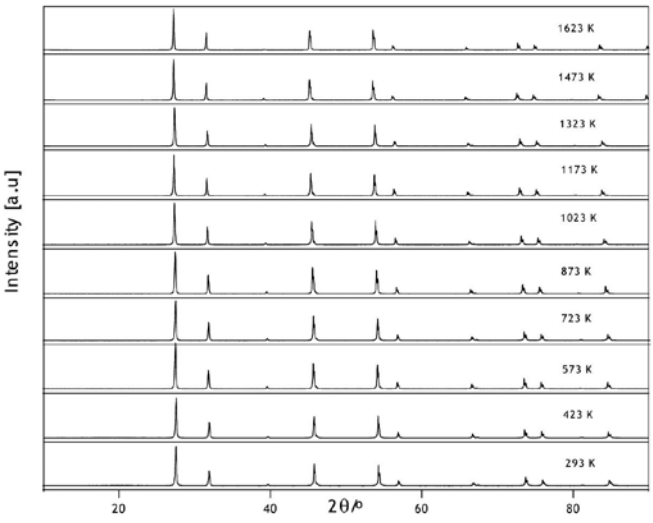

Fig. 1. XRD patterns of ThO_2-4 wt.% UO_2 at different temperatures

Simulation of thermal expansion behavior in ThO_2-PuO_2 system using ceria as a surrogate material for plutonia

The thermal expansion behavior of ThO_2-PuO_2 system is not well reported in literature. A lucid review of the thermophysical and thermodynamic properties of ThO_2, $Th_{1-y}U_yO_2$ and $Th_{1-y}Pu_yO_2$ was made by Bakker et al. [17], which revealed that the mixed oxides in the ThO_2-PuO_2 systems are very scantily reported in the literature. The main difficulties while investigating PuO_2-based systems are its high radioactivity and toxicity. One way to overcome this problem is the use of CeO_2 in place of PuO_2 as they both have quite similar physico-chemical properties viz., ionic size in octahedral and cubic coordination, melting points, standard enthalpy of formation and specific heat, etc. Typical physical properties of CeO_2 and ThO_2 are summarized in Table II, which reveals that CeO_2 is an ideal surrogate material to simulate thermophysical properties of PuO_2 and PuO_2-based systems [20]. About ten compositions in the $Th_{1-x}Ce_xO_2$ system were prepared by ceramic route, as described earlier. In order to ascertain the incorporation of Ce^{4+} into the lattice of ThO_2, the room temperature XRD patterns of ThO_2, CeO_2 and all the mixed oxides were refined. The observed gradual decrease in the lattice parameter as a function of Ce^{4+} concentration in $Th_{1-x}Ce_xO_2$ series can be attributed to the different ionic radii of Th^{4+} and Ce^{4+}, which is 1.05 and 0.90 Å, respectively, in eight fold coordination. The lattice thermal expansion behavior of these solid solutions was investigated by high temperature-XRD. It was observed that the doping of CeO_2 into ThO_2 has got a noticeable effect on its thermal expansion behavior. The increase in lattice thermal expansion coefficient (α_l) on going from ThO_2 to CeO_2 can be attributed to a relatively higher α_l value of CeO_2 which in turn can be correlated to its lower melting point as compared to that of ThO_2. The variation of average lattice thermal expansion coefficient as a function of composition, in $Th_{1-x}Ce_xO_2$ series, is shown in Fig. 2 and can also be represented as the following equation:

α_a (in ppm K^{-1}) = 9.54 + 1.74 x + 0.37 x^2 + 1.86 x^3 - 1.86 x^4 (where x is the Ce content)

Table II: The comparison of properties of ceria and plutonia

Property	CeO_2	PuO_2
Ionic size	Ce^{4+} = 0.87Å (in octahedral oordination) Ce^{4+} = 0.90Å (in cubic coordination)	Pu^{4+} = 0.86Å (in octahedral coordination) Pu^{4+} = 0.89Å (in cubic coordination)
Structure	Fluorite	Fluorite
M.P.	2873 K	2935 K
Density	7.30 g/cc	11.44 g/cc
Enthalpy (kJ/mol)	-1090.4	-1055.8
Specific heat (kJ/mol.K)	61.63	66.25
Entropy (J/mol.K)	62.30	66.13
$\alpha \times 10^6$ (K^{-1})	11.83	11.61

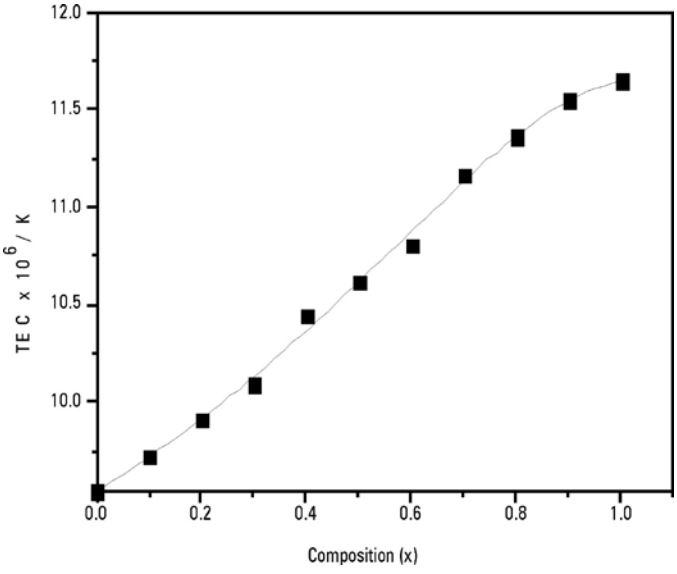

Fig.2: The a_a vs composition in $Th_{1-x}Ce_xO_2$

HT-XRD studies in ThO_2-M_2O_3 system (M = Nd^{3+}, Eu^{3+}, Gd^{3+}, Dy^{3+})

ThO_2-M_2O_3 system (M = Nd^{3+}, Eu^{3+}, Gd^{3+}, Dy^{3+}) is an important system from the point of view of several reasons viz., Nd is used as a burn up monitor in the spent fuel whereas Eu, Gd and Dy are commonly used as burnable neutron poisons, which are required for maintaining the controlled fission process in a nuclear reactor. Therefore, this system needs to be investigated. Based on XRD analysis, the phase relations in ThO_2-M_2O_3 system have been established. It was observed that the cubic fluorite type structures in $Th_{1-x}M_xO_{2-x/2}$ series (M = Nd^{3+}, Eu^{3+}, Gd^{3+} and Dy^{3+}) are retained till the compositions of $Th_{0.50}Nd_{0.50}O_{1.75}$, $Th_{0.50}Eu_{0.50}O_{1.75}$, $Th_{0.60}Gd_{0.40}O_{1.80}$ and $Th_{0.85}Dy_{0.15}O_{1.925}$ in the respective systems. It implies that while 50 mol% $NdO_{1.5}$ and $EuO_{1.5}$ can be incorporated into ThO_2 lattice, only 40 mol % $GdO_{1.5}$ and 15 mol % $DyO_{1.5}$ is soluble in ThO_2 lattice under the slow cooled conditions. The solubility behavior of Nd^{3+}, Eu^{3+}, Gd^{3+} and Dy^{3+} in the lattice of ThO_2 can be attributed to the ionic radii of host and guest ions. The ionic radii of Th^{4+}, Nd^{3+}, Eu^{3+}, Gd^{3+} and Dy^{3+} are 1.05 Å, 1.02 Å, 0.98 Å, 0.97 Å and 0.94 Å, respectively, in eight-fold coordination. As the difference between ionic radii of host and guest ions increases, the solubility limit decreases. The minimum solubility is in the system with largest difference in ionic radii of host and guest ions such as Th^{4+} and Dy^{3+}. At and beyond the compositions of $Th_{0.45}Nd_{0.55}O_{1.725}$, $Th_{0.45}Eu_{0.55}O_{1.725}$ $Th_{0.55}Gd_{0.45}O_{1.775}$ and $Th_{0.80}Dy_{0.20}O_{1.90}$, additional peaks started appearing which could be identified due to the respective rare-earth oxides.

The lattice thermal expansion studies of the single-phasic solid solutions as well as of Nd_2O_3, Eu_2O_3, Gd_2O_3 and Dy_2O_3 were carried out from room temperature to 1473 K. XRD pattern of each sample recorded at different temperatures was refined to determine the lattice parameter as a function of temperature. The cell parameters of the solid solutions and $MO_{1.5}$ compounds showed a nearly linear increase with increase in temperature. The lattice thermal expansion coefficients (α_a) of the solid solutions as evaluated from the cell parameters in the temperature range of 293-1123 K and 293-1473 K are given in Table III. It is evident from the table that the coefficients of average lattice thermal expansion of the solid solutions ThO_2-M_2O_3 system (M = Nd^{3+}, Eu^{3+}, Gd^{3+}, Dy^{3+}) decrease on going from Nd_2O_3 to Dy_2O_3, in the temperature ranges of investigation.

Table III: Coefficients of average lattice thermal expansion (α_a) of $Th_{1-x}M_xO_{2-x/2}$ (M = Nd^{3+}, Eu^{3+}, Gd^{3+} and Dy^{3+}) solid solutions

Sr. No.	Nominal Composition	α_a (x 10^6K^{-1}) (293-1473K)			
		M = Nd^{3+}	Eu^{3+}	Gd^{3+}	Dy^{3+}
1.	$Th_{1.0}M_{0.0}O_2$	9.55	9.55	9.55	9.55
2.	$Th_{0.90}M_{0.10}O_{1.95}$	10.60	9.41	9.41	9.27
3.	$Th_{0.85}M_{0.15}O_{1.925}$	-	-	-	9.13
4.	$Th_{0.80}M_{0.20}O_{1.90}$	10.76	9.26	9.11	-
5.	$Th_{0.70}M_{0.30}O_{1.85}$	10.91	8.81	8.83	-
6.	$Th_{0.60}M_{0.40}O_{1.80}$	11.06	8.68	8.68	
7.	$Th_{0.50}M_{0.50}O_{1.75}$	11.06	8.22	-	-

The observed trend of thermal expansion of the compounds appears to be more related to the ionic radii of the cations of the compounds. The thermal expansion characteristics of Nd_2O_3, Eu_2O_3, Gd_2O_3 and Dy_2O_3 seem to contribute significantly to the thermal expansion behavior of the solid solutions they form with thoria. The lattice thermal expansion coefficients of $Th_{1-x}M_xO_{2-x/2}$ (M = Nd^{3+}, Eu^{3+}, Gd^{3+} and Dy^{3+}) solid solutions with a given value of 'x' also show a decreasing trend on going from Nd^{3+} to Dy^{3+}. The noticeable difference in the thermal expansion behavior of the solid solutions of the systems is observed in ThO_2-Nd_2O_3 system. Except for this system, the linear and lattice thermal expansion coefficients of the solid solutions of other systems decrease progressively on increasing content of the respective substituent. The decrease in thermal expansion coefficient of these solid solutions on increasing the content of the dopants can be explained on the low values of thermal expansion coefficients of Eu_2O_3, Gd_2O_3 and Dy_2O_3, compared to that of ThO_2. Another reason could be that as the Eu^{3+}, Gd^{3+} and Dy^{3+} contents increase, defect concentration (oxygen vacancy) also increases, which can mask thermal expansion to some extent. These observations would be useful in knowing the chemical state of these rare earths in ThO_2 based nuclear fuels at different burn-ups and their influence on thermal expansion.

Conclusions

Thermal expansion behavior of several highly relevant thoria-based systems was elaborated in this article. High temperature XRD gives an intrinsic thermal expansion behavior, which unlike bulk thermal expansion by dilatometer, is not affected by micro-structure and bulk

density, etc. However, both the techniques have their own importance for investigating thermal expansion of solids. The readers may find more details from the publications from my group, cited in this article.

Acknowledgements

I very fondly remember two of my former colleagues, Late Shri B.R. Ambekar and Dr. M. D. Mathews, who were members of the team responsible for the work on thoria-based fuels. Acknowledgement is due to Radio Metallurgy Division, BARC for providing a few of the samples. I would like to place on records my sincere thanks to Dr. D. Das, Head, Chemistry Division and Dr. T. Mukherjee, Director, Chemistry Group, BARC.

References

1. R. M Hazen and C. T. Prewitt, *Am. Mineral.*, 62, (1977) 309.
2. Anil Kakodkar, "Shaping the third stage of Indian Nuclear Power Programme", presented at 12th Annual Conference of Indian Nuclear Society (INSAC-2001), Indore, India.
3. A. K. Tyagi and M. D. Mathews, *J. Nucl. Mater.*, 278 (2001)123.
4. R. D. Purohit, A. K. Tyagi, M. D. Mathews and S Saha, *J. Nucl. Mater.*, 280 (2000) 51.
5. M. D. Mathews, B. R. Ambekar, A. K. Tyagi, *J. Nucl. Mater.*, 280 (2000) 246.
6. R. D. Purohit, S. Saha and A. K. Tyagi, *J. Nucl. Mater.*, 288 (2001) 7.
7. M. D. Mathews, B. R. Ambekar and A. K. Tyagi, *J. Nucl. Mater.*, 288 (2001) 83.
8. A. K. Tyagi, M. D. Mathews, R. Ramachandran, *J. Nucl. Mater.*, 294 (2001) 198.
9. K. Tyagi, B. R. Ambekar, M. D. Mathews, *J. Alloys Comp.*, 337 (2002) 277.
10. R. D. Purohit, S. Saha and A. K. Tyagi, *J. Nucl. Mater.*, 323 (2003) 276.
11. M. D. Mathews, B. R. Ambekar and A. K. Tyagi, *J. Alloys Comp.*, 386 (2005) 234.
12. A. K. Tyagi, M. D. Mathews, B. R. Ambekar and R. Ramachandran, *Thermochimica Acta,* 421 (2004) 69.
13. M.D. Mathews, B.R. Ambekar and A.K. Tyagi, *J. Nucl. Mater.*, 341 (2005) 19.
14. M. D. Mathews, B. R. Ambekar and A. K. Tyagi, *J. Alloys & Comp.*, 386 (2005) 234.
15. M.D. Mathews, B.R. Ambekar and A.K. Tyagi, *Ceramic International,* 32 (2006) 609.
16. L. G. V. Uitert, H. M. O`Bryan, M. E. Lines, H. J. Guggenheim and G. Zydig, *Mater. Res. Bull.*, 12 (1977) 261.
17. K. Bakker, E.H.P. Cordfunke, R.J.M. Konings, R.P.C. Schram, *J. Nucl. Mater.*, 250 (1997) 1.

Dr. A. K. Tyagi *is presently Head, Solid State Chemistry Section, Chemistry Division, Bhabha Atomic Research Centre (BARC), Mumbai and also a Professor (Chemistry) at Homi Bhabha National Institute (HBNI). He joined BARC, Mumbai in 1986 through BARC-Training School. Since then he has been working in the field of Chemistry of nanomaterials, functional materials and nuclear materials. He was a Max-Planck Fellow at MPI, Stuttgart, Germany during 1995-96. In recognition of his work, Dr. Tyagi has been conferred with several prestigious awards such as Homi Bhabha Science & Technology Award, Gold Medal of Indian Nuclear Society, MRSI Medal, CRSI Medal, Dr. Laxmi Award by ISCAS, Rheometric Scientific-ITAS Award, and IANCAS-Dr.Tarun Datta Memorial Award, RD Desai Memorial Award of ICS, Rajib Goyal Prize in Chemical Sciences, DAE-SRC Outstanding Researcher Award and CRSI's CNR Rao National Prize for Chemical Sciences. He is a Fellow of Royal Society of Chemistry, UK (FRSC), National Academy of Sciences, India (FNASc) and Maharashtra Academy of Sciences (FMASc). He has been a visiting scientist to several countries like Germany, USA, Canada, France, Spain, Sweden, Portugal, Russia, Japan, Israel, China, Singapore and Malaysia*

Thermo-physical properties of alkaline earth silicate based glass/glass-ceramics for high temperature sealing applications

M. Goswami, P. Nandi, G. P. Kothiyal*
Glass and Advanced Ceramics Division,
Bhabha Atomic Research Centre, Mumbai - 400085
**Email: gpkoth@barc.gov.in*

Abstract

In this article, we present some of our results on thermo-physical properties of Ba/Ca-based alkaline earth silicate glasses/glass-ceramics for high temperature sealing application and their possible uses in solid oxide fuel cells (SOFCs). We have investigated different glass systems; however, we report here the results on two glass systems with the following base compositions (a) 35BaO-15CaO-5Al_2O_3-10B_2O_3-35SiO_2 (BCABS) and (b) 34BaO-10Al_2O_3-17B_2O_3-34SiO_2-5La_2O_3 (BABSL). High temperature characterization was carried out with the help of differential thermal analysis (DTA) and thermo-mechanical analysis (TMA) along with X-Ray diffractometry (XRD), scanning electron microscopy (SEM) and energy dispersive spectroscopy (EDS). In these systems, we have studied the effect of different additives (TiO_2, ZrO_2, Cr_2O_3 and P_2O_5) on thermo-physical and micro-structural properties leading to improved bonding characteristics with high ferritic steel (Crofer 22 APU). In addition, crystallization kinetics was also studied for BABSL system. BCABS glass having 2 mol% TiO_2 additive and BABSL with 1 mol% TiO_2 showed good bonding with Crofer 22 APU as compared to other additives. However, the BCABS seal with TiO_2 only showed long term chemical and thermal stability when heat treated at 800°C up to 1000 h.

Introduction

Solid oxide fuel cell (SOFC) is one of the most promising energy conversion devices that combine high efficiency, fuel flexibility and ability to combine heat and power applications. In comparison to the tubular design, planar design is considered to be superior due to its high current density and simple manufacturing process, but require sealant at the edge of the cell to prevent fuel leakage and air mixing at higher working temperatures [1-4]. Among the first and still most important sealants employed by planar stack builders are high temperature glasses and glass-ceramics and most common approach is to tailor the properties of the sealant material through fine tuning of glass composition. Many studies have been reported on glass and glass-ceramics based sealant materials to achieve desirable properties for SOFC application [5-9]. However, each system/category has its own drawbacks such as thermal expansion mismatch, high temperature stability or high chemical reactivity with other SOFC components. Alkaline earth silicate systems are considered among the potential systems for use as high temperature sealing materials and considerable work has been reported related to their synthesis and characterization [10-18].

In glass systems, thermo-physical properties are considered as function of the concentration and nature of constituents whereas in case of the glass-ceramics, thermo-physical properties are not only dependent upon the compositions but also on the crystallization heat treatment. A judicious choice of heat treatment, which is decided by means of thermal analysis techniques such as differential thermal analysis (DTA), is essential for optimum crystallization of the glasses [19-20]. The DTA data can also be used to measure the activation energy for crystallization and understand its mechanism (e.g., surface or bulk) [21]. In addition to DTA, thermal expansion coefficients (TEC), glass transition temperature (T_g) and dilatometric softening temperature (T_{ds}) of glasses and glass-ceramics can be measured by means of thermo-mechanical analysis (TMA). A combination of the thermal analysis techniques mentioned above along with structural characterization using XRD and SEM has been useful for improving the bonding characteristics.

In this paper, we present preparation and thermo-physical properties of BaO-CaO-Al_2O_3-B_2O_3-SiO_2 (BCABS) and BaO-Al_2O_3-B_2O_3-SiO_2-La_2O_3 (BABSL) glass systems with different additives. Glasses were characterized for their thermo-mechanical, crystallization kinetics, high temperature morphology, etc. Bonding/adhesion behavior of these glasses was investigated by fabricating seals with Crofer 22 APU interconnect. Microstructure at the interface, vacuum compatibility and high temperature stability of these seals were measured after heat treatment at 800°C for 1000 h.

Methodology

Glass preparation

The glasses with compositions (in mol %) 35BaO-15CaO-5Al_2O_3-8B_2O_3-35SiO_2-2A (BCABS), where (A =additive = ZrO_2, TiO_2, P_2O_5, or Cr_2O_3) and 34BaO-10Al_2O_3-17B_2O_3-34SiO_2-(5-x)La_2O_3-(x)TiO_2, where (x = 0, 1, 2, 3, 4 mol %) were prepared by the melt quench technique. Analytical grade precursors in the form of oxides/ nitrates/carbonates were mixed thoroughly and calcined in recrystallized alumina crucibles according to a heating schedule determined by the decomposition temperatures of the precursors. To ensure complete decomposition of nitrates and carbonates into their oxides, the batch was weighed before and after the calcination. The calcined batch was melted under ambient air at 1400-1450°C in a Pt-Rh crucible in a raising lowering hearth electric furnace (Model: OKAY, M/s Bysakh and Co., Kolkata) and held for 1-2 h for homogenization. The melt was poured into a pre-heated graphite mould, annealed at around 600 - 650°C for 3-4 h and thereafter slowly cooled down to room temperature.

Characterization

The vitreous nature of annealed glasses was verified by powder XRD (Philips PW1710 X-Ray Diffractometer with collimated Cu Kα radiation). Thermal properties like glass transition (T_g) and crystallization temperature (T_c) of the glass samples were measured using a TG-DTA system (SETARAM 92-15 TG/DTA) in the temperature range of 30-1000°C in argon atmosphere. Measurements were done on powdered glass samples using platinum standard and reference crucibles. Different heating rates (β = 10, 15, 20°C/min.) were used to calculate the activation energy of crystallization. Glass samples were transformed to glass-ceramics by controlled heat treatment for 10 h at their respective T_c obtained from the DTA data.

Thermal expansion coefficient (TEC) along with the dilatometric softening temperature (T_{ds}) and glass transition temperature (T_g) of the glass and glass-ceramics samples were determined using a thermo mechanical analyzer (Model: TMA 92, M/s SETARAM, France) in the range 30-1000°C using a silica probe in argon atmosphere. Flat circular discs of diameter 10 mm and thickness 3-4 mm were used for the experiments. The average TEC was calculated in the temperature range from 30 to 500°C.

Identification of various crystalline phases in glass-ceramics was carried out by powder XRD. Microstructures at the interfaces of seals and in glass-ceramics samples were investigated using SEM-EDS (Model SNE 3000M, SEC Eng, Korea). Prior to sealing experiments, to have an idea about sealing temperature, high temperature optical microscopy of these glasses was carried out up to 950°C using an optical microscope (Model BX60M, Olympus) having a hot stage. For these experiments glass sample in the form of powder was taken on a thin quartz disc and heated at the rate of 5°C/min. while monitoring the changes through a microscope and recording the images.

Seal fabrication

Sealing of different glasses with Crofer 22 APU alloy was carried out at temperatures between 950 and 1000°C employing the sandwich geometry. For this, slurry of fine glass powders was applied on Crofer 22 APU plate and then another equal size Crofer plate with a central hole and having a stainless steel (SS) extension tube welded for connection to vacuum system was placed on the top. A small load is placed on the top of it. This assembly was then heated in an inert atmosphere in a controlled manner with predetermined heating schedule to form seals.

Results and discussion

Thermo-physical studies

In this section, we shall illustrate the role of DTA and TMA in alliance with high temperature microscopy in the optimization of BCABS and BABSL glass composition suitable for seal fabrication with SOFC components. Fig. 1 and 2 show the DTA plots at constant rate of heating β = 10°C/min with different additives for BCABS and BABSL glass systems, respectively. Gradual endothermic shift with temperature indicates the glass transition (T_g) and exothermic peak indicates the crystallization temperature (T_c) as shown in figures. In Fig.1, no prominent exothermic peak is observed in the temperature range 30-1000°C for TiO_2, P_2O_5 and ZrO_2 substituted BCABS samples. This indicates that the crystallization process could not be initiated in these samples. However, Cr_2O_3 substituted sample showed a strong exotherm around 725°C, indicating a crystallization tendency. Glass transition temperatures extracted from DTA plots are found comparable with TMA data.

In Fig. 2, Glass transition temperature of the investigated compositions is nearly unchanged because of similar glass network structure. Glass composition x = 0, which is nucleated by La_2O_3, shows higher T_c. With increasing TiO_2 concentration, T_c initially decreases and then increases. The crystalline peak becomes stronger with the increasing TiO_2 content. TiO_2 enhanced the nucleation and thus increased the temperature for maximum nucleation rate thereby resulting in increased crystallization temperature. Similar results were reported in Ca-La-B-O glass system with varying TiO_2 content [22-24]. In BABSL glass, both La_2O_3

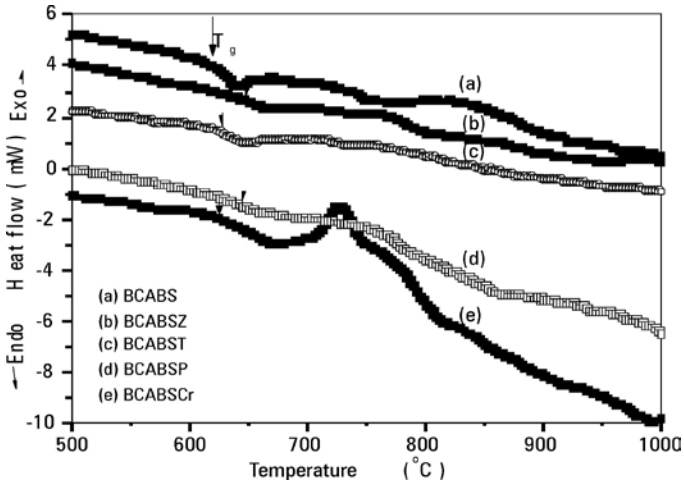

Fig.1 DTA plot for BCABS glass samples with different additives.

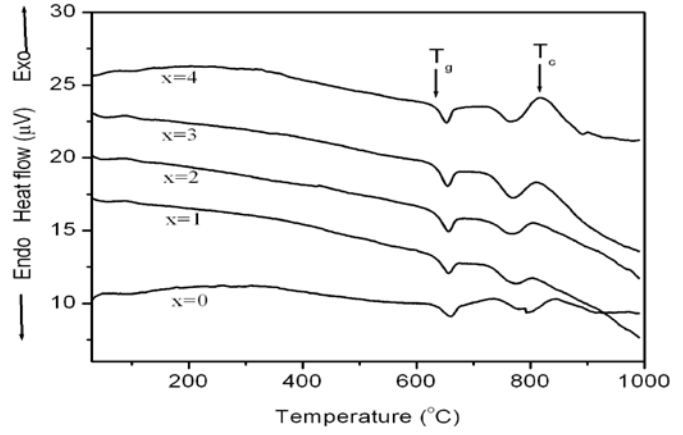

Fig. 2. DTA plot of the BABSL glass samples with different TiO_2 content.

and TiO_2 are acting as nucleating agent and helping in crystallization of these glasses.

Table 1 summarizes TEC, T_g and T_{ds} for BCABS glasses with different additives. Average TEC of these glasses was found to be in the range 10.34 - 12.81 × 10^{-6}/°C (30 - 500°C). TEC and T_g values for samples having ZrO_2, are found to be higher than those of samples containing other additives.

Table 1 Thermo-physical parameters for BCABS glass samples with various additives.

Samples	TEC (30-500°C)	T_g (°C)	T_{ds} (°C)
BCAB(without substituent)	11.9 × 10^{-6}/°C	619	665
BCABST (TiO_2)	11.58 × 10^{-6}/°C	629	669
BCABSP (P_2O_5)	12.04 × 10^{-6}/°C	641	660
BCABSZ (ZrO_2)	12.81 × 10^{-6}/°C	652	670
BCABSCr (Cr_2O_3)	11.34 × 10^{-6}/°C	632	678

Table 2 summarizes TEC, T_g, T_{ds} for BABSL glasses with varying TiO_2 content. Glass composition x = 0 with maximum La_2O_3 concentration has the highest T_{ds}. TEC of the glasses showed very little variation and found to be in the range 10.3 - 9.9 × 10^{-6}/°C (30 - 500°C).

Table 2 Thermo-physical parameters for BABSL glasses with different TiO_2 concentrations

TiO_2 content (x) in mol%	Differential Thermal Analysis		Thermo Mechanical Analysis		
	T_c (°C)	Activation Energy (E_a) (kJ mol^{-1})	T_g (°C)	T_{ds} (°C)	TEC (30 – 500°C) (± 0.2)
0	838	197	644	680	10.3 × 10^{-6}/°C
1	804	340	643	672	10.3 × 10^{-6}/°C
2	805	324	640	671	10.1 × 10^{-6}/°C
3	811	311	645	671	10.1 × 10^{-6}/°C
4	816	216	648	671	9.9 × 10^{-6}/°C

BABSL glass system showed strong crystallization peaks (Fig. 2) indicating clear tendency towards devitrification, which necessitates the study of crystallization kinetics in order to understand the devitrification phenomenon of these glasses. Crystallization kinetics of these glasses was investigated by DTA using different heating rates (β). In general, it has been observed that T_c increases with increasing β. The activation energy of crystallization (E_a) can be obtained from the modified Kissinger equation:

$$\ln\left(\frac{T_c^2}{\beta^n}\right) = m\frac{E_a}{RT_c} + \text{Constant} \qquad (1)$$

where, 'n' is the Avrami constant and 'm' is the crystal growth dimensionality. 'R' is the universal gas constant. In the present study, we have taken n = m = 1, which is

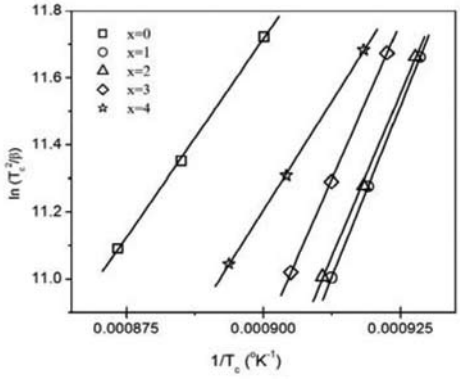

Fig. 3. Activation energy of crystallization of BABSL glasses calculated from the linear fit shown in solid lines with the experimental data points drawn in symbols.

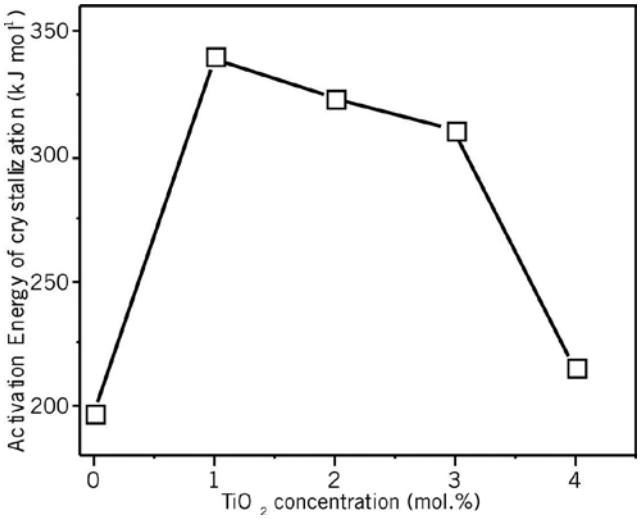

Fig. 4. Variation in activation energy with different TiO_2 content in BABSL glass

the case for surface crystallization. T_c data plotted for different heating rates (β) and their straight line fitting using equation 1 are shown in Fig. 3.

Calculated activation energies (E_a) are reported in Table 2. Activation energy relates to the rate of crystallization. Composition with x = 1 is having the higher activation energy, therefore have the slower rate of crystallization. Activation energy of crystallization initially increases and then decreases with increasing TiO_2 concentration.

Phase evolution at high temperature

As BCABS glasses are very stable towards devitrification, prolonged heat treatment up to a maximum of 300 h at 800°C was given to see the systematic phase evolution with time. Fig. 5a shows the room temperature XRD patterns of TiO_2 added BCABS glass sample, heat treated at 800°C for different durations. XRD patterns of the samples remained unchanged up to 10 h of heat treatment. After heat treatment of 100 h, barium orthosilicate ($BaSi_2O_5$) developed as a minor crystalline phase whereas $Ba_{1.5}Ca_{0.5}SiO_4$ and $BaSi_2O_5$, phases were developed after 300 h of heat treatment. It showed a marginal change in TEC and values were found to vary in the range of 11.67 and 11.02 × 10^{-6}/ °C with variation of duration of heat treatment. Since TEC values of these developed phases are nearly the same to that of the base glass [5], the overall TEC did not show appreciable change after heat treatment. In case of BCABSP sample, XRD results revealed the formation of $BaSi_2O_5$ and $BaAl_2Si_2O_8$ phases after heat treatment of 300 h and for the sample with Cr_2O_3 additive, XRD confirmed the presence of $Ba_2(CrO_4)$ along with $BaSi_3O_8$, $BaSiO_3$, $BaAl_2Si_2O_8$ phases (Fig 5b). As $BaSi_2O_5$ (TEC = 14 × 10^{-6}/°C) and Ba_2CrO_4 (TEC = 16 - 18 × 10^{-6}/°C) phases have higher TEC and $BaAl_2Si_2O_8$ (TEC = 7 - 8 × 10^{-6}/°C) has a comparatively lower value, the overall TEC of the samples did not change appreciably even after heat treatment at 800°C for 300 h.

Fig. 6 shows the X-Ray diffraction patterns of BABSL glass samples having different TiO2 content, heat treated for 10 h at their respective crystallization temperatures. XRD pattern showed the formation of only $BaSi_2O_5$ phase for composition x = 0, 1 while others showed co-existence of $BaSi_2O_5$ and BaB_2O_4 phases (Fig. 6). TEC is found to

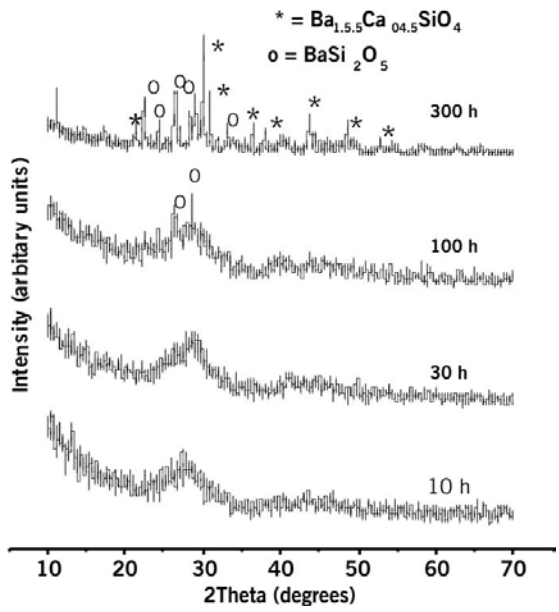

Fig. 5a. XRD patterns of TiO_2 added BCABS glass samples heat treated at 800°C for different durations.

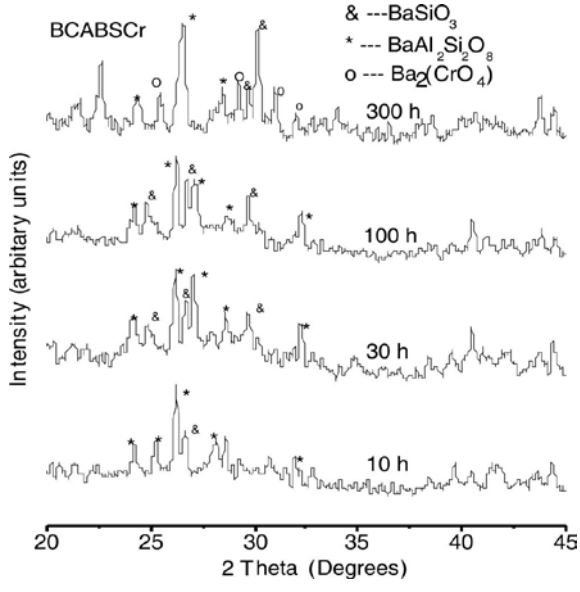

Fig. 5b. XRD patterns of Cr_2O_3 added BCABS glass samples heat treated at 800°C for different durations

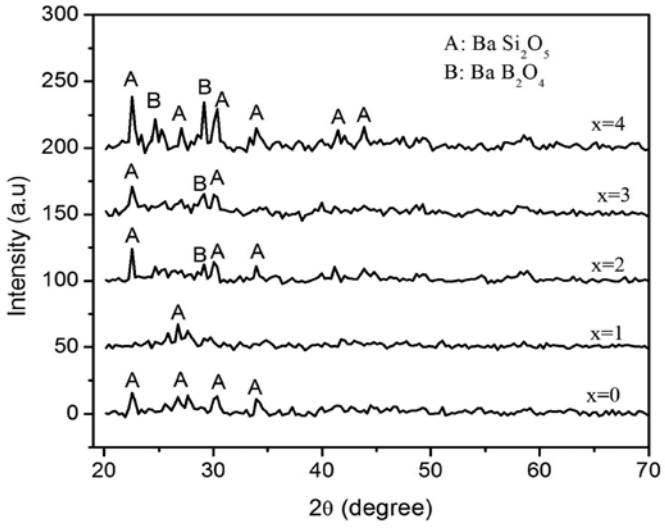

Fig. 6. XRD patterns of the BABSL glasses heat treated for 10 h at their respective T_c.

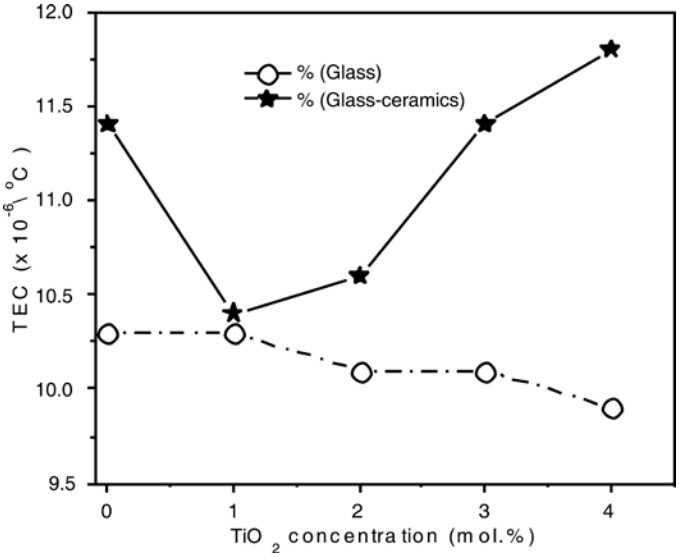

Fig. 7. Variation of TEC of BABSL glass and glass-ceramics with different TiO_2 content.

increase in glass samples after the heat treatment. Variation of TEC in glass-ceramics samples is shown in Fig. 7. With the increase in TiO_2 concentration, TEC of the glass-ceramics initially decreases and then increase. There are increments in TEC after the formation of glass-ceramics due to the evolution of crystalline phases with higher TEC and their relative crystalline volume. The observed increase in TEC of glass-ceramics is because of higher TEC of barium silicate and barium borate phase emergence and their relative crystalline concentrations present in these glass-ceramics. Interestingly, glass composition (x = 1) with highest activation energy shows the lowest increment in TEC as it has minimum crystalline volume among the studied compositions.

High temperature microscopy

Fig. 8 shows representative images collected for BCABS glass having TiO_2 additive, at different temperatures on a hot stage microscope. These images show maximum shrinkage at about 860°C and melting at ~ 950°C for the powdered glass samples. Using the above data as a guide, the optimum sealing temperature was found to be 990°C for TiO_2 added BCABS. Similarly, for other additives, the shrinkage patterns were determined and temperatures were optimized for seal fabrication.

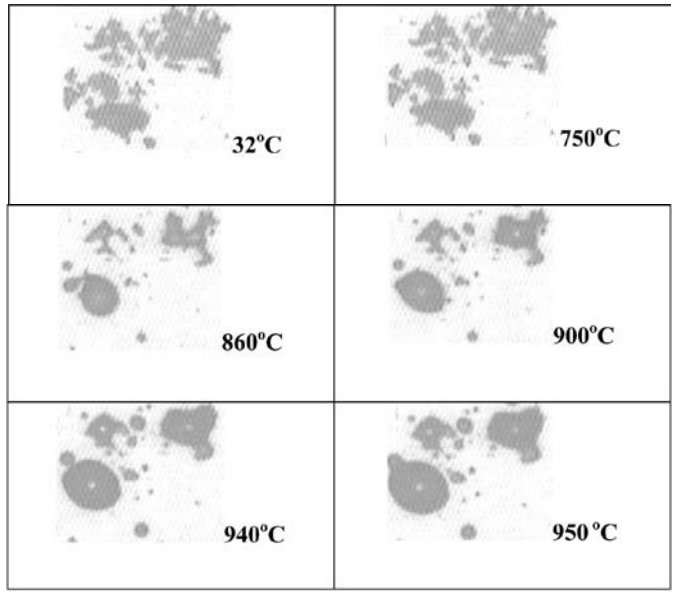

Fig. 8. Optical microscope images for BCABST glass sample at various temperatures.

It is suggested that glass with lower crystallization tendency is favourable because, after long thermal cycles the crystalline phase will squeeze out the glass matrix causing the break down of a seal. Considering thermo-physical and crystallization kinetics, seals fabricated with Crofer 22 APU were characterized for their vacuum compatibility and interface microstructure. To see the bonding properties of glasses under investigation, button type seals were fabricated with Crofer 22 APU in the temperature range of 950 - 1000°C. Seal fabricated with TiO_2 added BCABS glass was only found to withstand a vacuum of 10^{-6} torr at 800°C after heat treatment at 800°C for 1000 h. To understand the behavior of the glass as well as seal at high temperature, detailed thermo-physical, interface and structural studies are presented below.

Interface studies

Fig. 9 shows the XRD patterns of TiO_2 added BCABS glass samples removed from the heat treated seals interfaces after heat treatment at 800°C for 300 h (mentioned

as seal in Fig. 9). For comparison purpose, XRD patterns of the as-prepared glass samples heat treated under identical conditions are also plotted (mentioned as glass in Fig. 9) along with that of seal. The major phase is identified as $BaSi_2O_5$ along with $Ba_{1.5}Ca_{0.5}SiO_4$ (PCPDF:17-0930) at the interface region in the seal. Whereas in case of as-prepared glass, it is just reverse and the major crystalline phase has been identified as $Ba_{1.5}Ca_{0.5}SiO_4$ along with $BaSi_2O_5$. As the TEC of these phases are in the order of their base glass, the thermal and mechanical stability of these seals remain intact even after prolonged heat treatment.

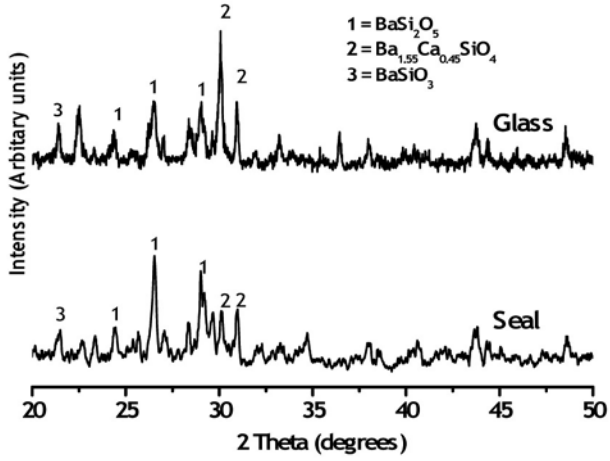

Fig. 9 XRD patterns of glasses removed from the heat treated seal interface and as-prepared TiO_2 added BCABS glass.

Fig. 10a shows the secondary electron images of BCABST glass/Crofer 22 APU interfaces of the seals heat treated at 800°C for 1000 h. From these figures, formation of two different crystalline phases promoted by the presence of interconnect material in the glass matrix is clearly observed. These crystalline phases are identified as Barium rich phase with brighter region and Silica rich phases with relatively darker region. These crystallites are of size range ~2 - 10 microns. Elemental line scans for the seal, heat treated at 800°C for 1000 h are shown in Fig. 10b. It shows enrichment of Cr and Mn at the interface along with inter-diffusion of Fe, Cr, Ba, Ti, and Ca across the boundary. The Cr-Mn enrichment at the interface may lead to the formation of a Cr-Mn spinel thereby helping in good bonding. It was reported that the presence of Cr-Mn spinel acts like an active barrier for diffusion of elements across the boundary [4].

Fig. 11a show the back scattered electron images of seal fabricated with BABSL with x=1. BSE image shows grey area rich in Ba, Si and bright areas rich in La, Al thought to be the crystalline phase and glassy phase respectively. The microstructure for x=1 is rather well formed by self healing process with sharp interface boundary. Elemental line scans across the interface are shown in Fig. 11(b). Relatively small amount of Cr enrichment observed after 10 h of heat treatment. Long term stability test with x=1 glass is underway to estimate its reliability of this composition for high temperature sealing.

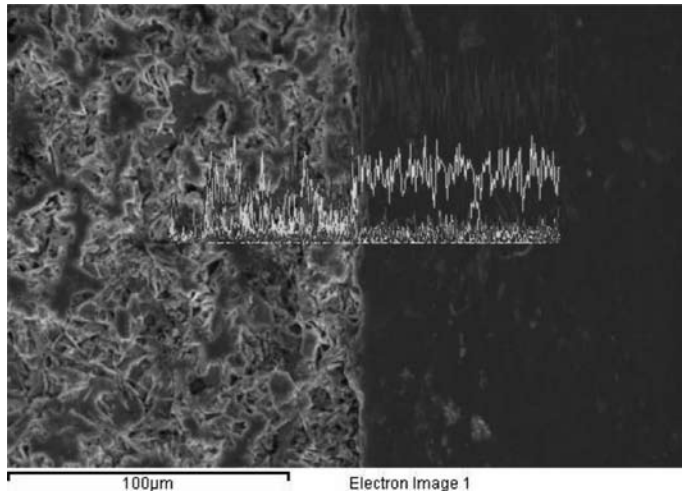

Fig.10a Microstructures at the interface of the BCABST glasses with Crofer 22 seals after heat treatment at 800°C for 500 h.

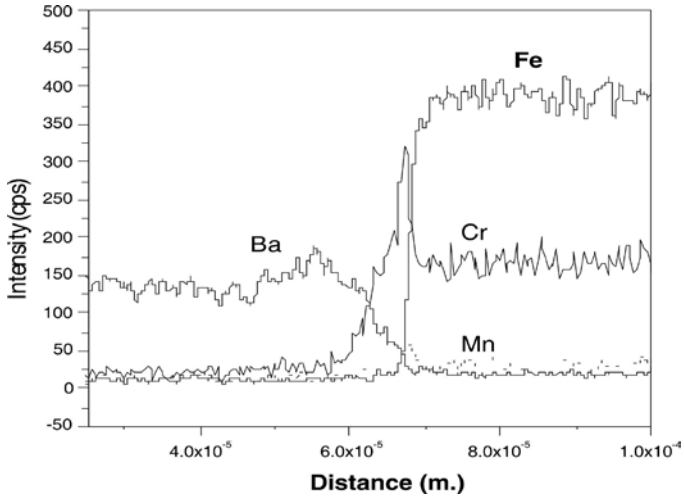

Fig.10b Elemental line scan across the interface of BCABST glasses with Crofer 22 APU seal after heat treatment at 800°C for 500 h.

Leak testing for the seals fabricated was carried out and seals were found to withstand a vacuum of 10^{-6} torr at room temperature. Further in-situ leak testing of the seals was also carried out at different temperatures up to 800°C by holding them at a desired temperature and monitoring the changes in pressure gauge. Seals fabricated with TiO_2 added BCABS and BABSL with x=1 glasses found to withstand a vacuum of 10^{-6} torr up to 800°C.To see the high temperature stability of these seals, they were kept at 800°C for different durations up to maximum1000 h

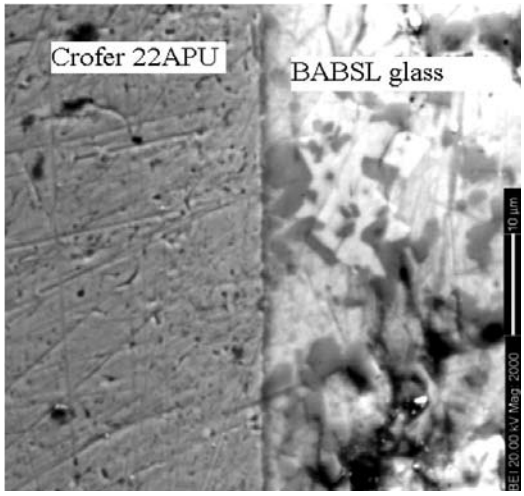

Fig.11a Microstructures at the interfaces of the BABSL glasses with Crofer 22 APU seals after heat treatment at 800°C for 10 h.

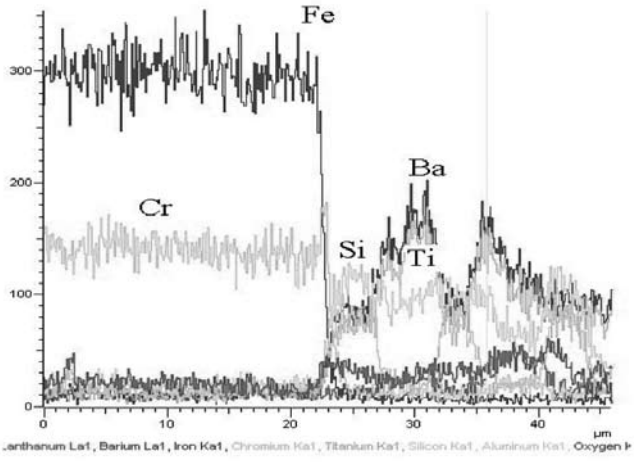

Fig.11b Elemental line scan across the interfaces of BABSL glasses with Crofer 22 APU seal after heat treatment at 800°C for 10h.

and tested again for vacuum at room temperature as well as elevated temperatures. Only the seal fabricated with 2mol% TiO_2 added BCABS glass was found to withstand a vacuum of 10^{-6} torr indicating their integrity up to 800°C after heat treatment at 800°C for 1000h.

Conclusions

35BaO-15CaO-5Al_2O_3-10B_2O_3-35SiO_2 and 34BaO-10Al_2O_3-17B_2O_3-34SiO_2-5La_2O_3, with different additives were prepared by melt–quench technique. In BCABS glass samples, DTA studies showed that, there is no exothermic peak for 2 mol. % of ZrO_2, P_2O_5 and TiO_2, but for 2 mol. % of Cr_2O_3, whereas BABSL samples showed strong exothermic peak showing tendency toward crystallization. In glass samples TEC remained nearly unchanged for both the system with different additives. On the other hand, TEC was found to increase in BABSL glasses after heat treatment due to formation of crystalline phases like $BaSi_2O_5$ and BaB_2O_4 with higher TEC and their relative concentration. TEC of TiO_2 added BCABS glass remained nearly unchanged after heat treatment at 800°C for 300h. BCABS glass with lower crystallisation tendency was found suitable for long term uses at high temperature compared to BABSL glasses. XRD measurements on as prepared TiO_2 added BCABS glasses as well as glasses removed from the interface of the seals after heat treatment at 800°C for 300h showed that the nature of phases formed were same but with different volume fraction. Seals fabricated with TiO_2 added BCABS glass and BABSL glass with x=1(1 mol.% TiO_2) with Crofer 22APU showed good bonding and withstood a vacuum of 10^{-6} torr after heat treatment at 800°C for 500h but only the seal fabricated with TiO_2 added BCABS glass was found to maintain good chemical and thermal stability at 800°C even after heat treatment at 800°C for 1000h.

Acknowledgements

Authors wish to thank Dr A. K. Suri for encouragements and support to this work. We would like to thank Smt Shobha Sinaravelan, Smt Aparna Patil and Shri A Sarkar for their help in various studies. Technical help from Shri Wagh and Shri R S Nair is gratefully acknowledged.

References

1. N. Q Minh, *Solid State Ionics,* 174 (2004) 271.
2. S.C. Singhal, *Solid State Ionics,* 152-153 (2003) 405.
3. N. Q. Minh. *J. Am. Ceram. Soc.,* 76 (1993) 563.
4. S. P. Badwal, *Solid State Ionics,* 143 (2000) 39.
5. J. W. Fergus, *J. Power Sources,* 147 (2005) 46.
6. M. K. Mahapatra, K Lu, *J. Power Sources,* 195 (2010) 7129.
7. A. Ananthanarayanan, G. P. Kothiyal, L. Montagne, G. Tricot and B. Revel, *Mater. Chem. Phys.,* 130 (2011) 880.
8. K. Sharma, G.P. Kothiyal, L. Montagne, F. O. Méar, B. Revel, *Int. J. Hyd. Eng.,* 2012, (in press)
9. P. Kothiyal, Madhumita Goswami, Babita Tiwari, Kuldeep Sharma, A. Ananthanarayanan and Lionel Montagne, *Chinese J. Adv. Ceram.,*(2012) Review paper (In press).
10. K. D. Meinhardt , D. S. Kim ChouYS, K.S. Weil, *J. Power Sources,* 182 (2008) 188.
11. W. Liu, S. Xin, A. Khaleel Mohammad, *J. Power Sources,* 185 (2008) 1193.
12. Z. Yang, J.W. Stevenson, K.D. Meinhardt, *Solid State Ionics,* 160 (2003) 213.
13. K. Eichler, G. Solow, P. Ostchik, W. Schaffrath, *J. Eur. Ceram. Soc.,* 19 (1999) 1101.
14. S. B. Sohn, S. Y. Choi, G. H. Kim, H. S. Song, G. D. Kim, *J. Non-Cryst. Solids,* 297 (2002)
15. 103.
16. M. J. Pascual, A. Guillet, A. Duran, *J. Power Sources,* 16 9(2007) 40.

17. V.A.C. Haanappel, V. Shemet, I. C. Vinke, W.J. Quadakkers, *J. Power Sources,* 141 (2005) 102.
18. Saswati Ghosh, A. Das Sharma, P. Kundu, S. Mahanty, R.N. Basu, *J. Non-Cryst. Solids,* 354 (2008) 4081.
19. S. Ghosh, A. Das Sharma, K. Mukhopadhyay, P. Kundu, R. N. Basu, *Int. J. Hyd. Energy,* 35 (2010) 272.
20. Wen, X. Zheng and L. Song, *Acta. Mater.,* 55 (2007) 3583.
21. X. Zheng, G. Wen, L. Song and X. X. Huang, *Acta Mater.*,56 (2008) 549.
22. X. Guo, H. Yang, C. Han, F. Song, *Thermochim. Acta,* 444 (2006) 201.
23. B. Tiwari, V. Sudarshan, A. Dixit, G. P. Kothiyal, *J. Am. Ceram. Soc.*, 94 (2011) 1440.
24. Kaushik Biswas, Atul D. Sontakke, K. Annapurna, *J. Alloys Comp.* 489 (2010) 493.
25. A. Bhargava, J.E. Shelby, R.L. Snyder, *J. Non-Cryst. Solids,*102 (1988) 136.

Dr. Madhumita Goswami *joined BARC in 1997 after graduating from 40th Batch (Chemistry) Training School. She is involved in the R&D works on various oxide glass and glass-ceramics for different applications. She completed PhD (Chemistry) on "Physico-chemical and structural aspects of oxide glass and glass-ceramics" from University of Mumbai on 2006. She also worked as a postdoctoral research fellow at Ecole Nationale Suprieure de Chimie de Lille, University of Science & Technology of Lille, France on the topic "Preparation of P_2O_5 containing glass ceramics for application in solid oxide fuel cell and characterization by using Solid State NMR". Currently she is involved in development work of glass/glass- ceramics for optical applications and use as host materials for divitrification radioactive wastes.*

Dr. Purnananda Nandi *received B.Sc. (Physics honors) and M.Sc. (Physics) degrees from Visva-Bharati University, Santiniketan. Then he did Ph.D in Physics from Indian Institute of Technology Guwahati. During his PhD he was involved in the study of the spectroscopic properties of rare-earth doped glasses, nonlinear optical properties of nanocluster embedded glasses and fabrication of femtosecond laser written channel waveguides for lasers and optical amplifiers. After that he moved to Centre for Photonics and Photonic Materials, University of Bath, UK, as a research officer working on fabrication and characterization of photonics crystals fibers. He was awarded prestigious DAE-BRNS KSKRA fellowship on 2010 (21st batch) and joined the Glass and Advanced Ceramics Division, BARC. Currently he is working on development glass/glass-ceramics for high temperature sealing and optical application.*

Prof. (Dr) G P Kothiyal, *Outstanding Scientist and Head, Glass and Advanced Ceramics Division, Bhabha Atomic Research Centre (BARC) has graduated from 13th batch (Physics) of BARC Training School. He has contributed very significantly in both science and technology areas. While spearheading the programme on special glasses and glass-ceramics, he has produced them with designed/tailored properties and delivered for use in nuclear, laser, defense and space applications. He has major areas of specialization in Glasses, Glass-ceramics & advanced Ceramics, Single crystal growth by vapour and melt growth, Thin film (crystalline and amorphous) growth by chemical deposition, conventional vapour phase as well as molecular beam epitaxy techniques, glass based devices/gadgets like Flash lamps, DC arc lamp, ionization gauges, glass-to-metal seals etc. He has published more than 130 research papers in peer reviewed journals. He is PhD guide at the Mumbai University and Homi Bhabha National Institute, Mumbai. He is recipient of several awards including DAE Group Achievement Award 2009, INS science Communication Award for the year 2009, MRSI Medal lecture Award 2002. He is MRSI subject group Chairman for Ceramics and Glass and secretary MRSI Mumbai Chapter. He has visited many overseas Laboratories in USA, France, Portugal, China, Singapore, Spain, Poland, etc.*

Printed by:
Ebenezer Printing House
Unit No. 5 & 11, 2nd Floor, Hind Service Industries
Veer Savarkar Marg, Shivaji Park Sea-Face, Dadar (W), Mumbai - 400 028
Tel.: 2446 2632 / 2446 3872 Tel Fax: 2444 9765
Email : eph@vsnl.com / outworkeph@gmail.com

In this issue

Feature Articles

Society for Materials Chemistry

C/o. Chemistry Division Bhabha Atomic Research Centre, Trombay, Mumbai, 400 085 (India)

E-mail: socmatchem@gmail.com,

Tel: +91-22-25592001